INT. J. REMOTE SENSING, 2002, VOL. 23, NO. 20, 4403–4438

Astronaut-acquired orbital photographs as digital data for remote sensing: spatial resolution

JULIE A. ROBINSON†*, DAVID L. AMSBURY‡,
DONN A. LIDDLE† and CYNTHIA A. EVANS†

†Earth Sciences and Image Analysis Laboratory, NASA Johnson Space Center and Lockheed Martin Space Operations, 2400 NASA Road 1, C23, Houston, TX 77058, USA
‡128 Homestead, Kerrville, TX 78028, USA

(*Received 15 November 2000; in final form 9 August 2001)*
Web Links Updated 02/26/2015

Abstract. Astronaut-acquired orbital photographs (astronaut photographs) are a useful complement to images taken by orbiting satellites. They are in the public domain, and have been particularly useful for scientists in developing countries, as supplementary low-cloud data, and for studies requiring large numbers of images. Depending on camera, lens and look angle, digitized astronaut photographs can have pixel sizes representing areas on the Earth as small as 10 m or less, although most photographs suitable for digital remote sensing have pixel sizes between 30 m and 60 m. The objective of this paper is to provide a practical reference for scientists in a variety of disciplines who want to use astronaut photographs as remote sensing data. The characteristics of astronaut photography systems that influence spatial resolution are detailed and previous image acquisitions relative to these elements are summarized. Methods are presented for estimating ground coverage under three different levels of assumptions, to meet accuracy needs of different users. Of the more than 375 000 photographs taken to date, at least half have the potential to be used as a source of digital remote sensing data.

1. Introduction

1.1. *Overview of NASA astronaut photography*

Astronaut photography of Earth is produced and archived by the National Aeronautics & Space Administration (NASA) and provides an important record of the state of the Earth that has not been used to its potential (Lulla *et al.* 1996). The practice was the foundation for the development of other forms of orbital remote sensing (Lowman 1999). Although the geometry is more complex than that of a vertical aerial photograph, astronaut photographs still provide information that can be interpreted by knowledgeable observers (Ring and Eyre 1983, Lowman 1985, Rasher and Weaver 1990, Drury 1993, Campbell 1996: 121–156, Arnold 1997).

Official NASA campaigns of terrain, ocean, and atmospheric photography were carried out during the Gemini missions (Underwood 1967, Lowman and Tiedemann

*email: julie.a.robinson@nasa.gov

International Journal of Remote Sensing
ISSN 0143-1161 print/ISSN 1366-5901 online © 2002 US Crown
http://www.tandf.co.uk/journals
DOI: 10.1080/01431160110107798

1971), the Earth-orbiting Apollo missions (Colwell 1971), the Apollo-Soyuz mission (El-Baz 1977, El-Baz and Warner 1979), Skylab (NASA 1974, Wilmarth *et al.* 1977), a few Shuttle missions (e.g. the two Space Radar Laboratory missions of 1994, Jones *et al.* 1996), and the Shuttle-*Mir* missions (Evans *et al.* 2000). Extensive training in photography is available to members of all flight crews, during their general training period and during intensive training for specific missions (Jones *et al.* 1996). Most photographs have been taken by astronauts on a time-available basis. Astronaut photographs are thus a subset of the potential scenes, selected both by opportunity (orbital parameters, lighting, and crew workloads and schedules) and by the training, experience, and interest of the photographers.

As remote sensing and geographic information systems have become more widely available tools, we have collaborated with a number of scientists interested in using astronaut photography for quantitative remote sensing applications. Digitized images from film are suitable for geometric rectification and image enhancement followed by classification and other remote sensing techniques (Lulla and Helfert 1989, Mohler *et al.* 1989, Helfert *et al.* 1990, Lulla *et al.* 1991, Eckardt *et al.* 2000, Robinson *et al.* 2000a, 2000c and in press, Webb *et al.* in press). The photographs are in the public domain, thus, they provide a low-cost alternative data source for cases where commercial imagery cannot be acquired. Such cases often include studies in developing countries, in areas that have not usually been targets for major satellites, needing supplemental low-cloud data, requiring a time series, or requiring a large number of images.

1.2. *Extent of the dataset*

As of 30 September 1999, 378 461 frames were included in the photograph database (Office of Earth Sciences 2000) comprising 99 missions from Mercury 3 (21 July 1961) through STS-96 (27 May to 6 June 1999). The database was reviewed, removing photographs that were deemed unsuitable for remote sensing analysis because they were not Earth-looking (no entry for tilt angle), had no estimated focal length, were over- or underexposed, or were taken at oblique tilt angles (further discussion of these characteristics follows). The remaining 190 911 frames (50.4% of the records present in the database) represent photographs that are potentially suitable for remote sensing data. As the database is always having new photography added, statistics can be updated on request using the web link 'Summary of Database Contents' at the *Gateway to Astronaut Photography of Earth* (Office of Earth Sciences 2000).

1.3. *Objectives*

The overall purpose of this paper is to provide understanding of the properties of astronaut-acquired orbital photographs to help scientists evaluate their applicability for digital remote sensing. Previous general descriptions of astronaut photography have been much less extensive and have tended to focus on numbers of photographs taken and geographic coverage, and emphasized interpretative applications (Helfert and Wood 1989, Lulla *et al.* 1993, 1994, 1996). By providing a unique compilation of the background information necessary to extend the use of astronaut photography beyond interpretation to rigorous analysis, it is hoped to provide a resource for scientists who could use this data in a variety of disciplines. In keeping with a potential interdisciplinary audience, we have tried to provide sufficient background information for scientists who do not have extensive training in remote sensing.

We focus on spatial resolution because it is one of the most important factors

determining the suitability of an image for a remote sensing objective. In remote sensing literature, spatial resolution for aerial photography is often treated very differently from spatial resolution of multispectral scanning sensors. To provide sufficient background for a discussion of spatial resolution for a data source that shares properties with both aerial photography and satellite remote sensing, we first summarize the ways that spatial resolution is typically quantified for aerial photography and satellite remote sensors.

Given this background information, we (1) describe and illustrate factors that influence the spatial resolution of astronaut photographs, (2) show examples of estimating spatial resolution for a variety of photographs in a way that will enable users to make these calculations whether or not they have a background in photogrammetry, and (3) compare spatial resolution of digital data extracted from astronaut photographs to data obtained from other satellites.

2. Background—Spatial resolution of imaging systems

Spatial resolution is a fundamental property of any imaging system used to collect remote sensing data, and directly determines the spatial scale of the resultant information. *Resolution* seems intuitively obvious, but its technical definition and precise application in remote sensing have been complex. For example, Townshend (1980) summarized 13 different ways to estimate the resolving power of the Landsat MultiSpectral Scanner (MSS). Simonett (1983, p. 20) stated 'In the simplest case, spatial resolution may be defined as the minimum distance between two objects that a sensor can record distinctly...[but] it is the format of the sensor system that determines how spatial resolution is measured'. By focusing attention on the properties of the system (and not the images acquired) this definition can be applied to a variety of types of images provided by different systems. In order to provide as complete a treatment as possible, background is provided on several views of spatial resolution that are relevant when considering the spatial resolution of astronaut photography.

2.1. *Ground resolved distance*

Photogrammetrists were measuring spatial resolution of aerial photographs using empirical methods long before the first scanning sensor was placed in orbit. These methods integrated properties of the imaging system with the other external factors that determine spatial resolution. Ground resolved distance (GRD) is the parameter of most interest, because it measures the applicability of an image to a specific task. The GRD of an image is defined as the dimensions of the smallest discernible object. The GRD is a function of geometry (altitude, focal length of optics), equipment (internal system spatial resolution of the camera or scanner) and also on reflectance characteristics of the object compared to its surroundings (contrast).

Performance of a film, film and camera, or deployed aerial photography system is measured empirically using standard targets that consist of black-and-white bars of graduated widths and spacings (figure 6–9 in Slater *et al.* 1983). The area-weighted average resolution (AWAR) in $\mathrm{lp\,mm^{-1}}$ (line pairs $\mathrm{mm^{-1}}$) at the film plane is determined by measuring the smallest set of line pairs that can be discriminated on an original film negative or transparency. Line pairs are quoted because it is necessary to discriminate between one object and another, to detect it and measure it.

Film resolving power (in $\mathrm{lp\,mm^{-1}}$) is measured by manufacturers under standard photographic conditions (Smith and Anson 1968, Eastman Kodak Company 1998)

at high contrast (object/background ratio 1000/1) and low contrast (object/background ratio 1.6/1). Most terrestrial surfaces recorded from orbit are low contrast, for the purpose of estimating resolving power of film. Kodak no longer measures film resolving power for non-aerial photographic films (Karen Teitelbaum, Eastman Kodak Company, personal communication), including films that NASA routinely uses for Earth photography.

AWAR can be measured for the static case of film and camera, or for the camera–aircraft system in motion. For example, AWAR for the National Aerial Photography Program includes effects of the lens, resolving power of original film, image blur due to aircraft motion, and spatial resolution of duplicating film (Light 1996). Given AWAR for a system in motion, the GRD can be calculated by trigonometry (see equation (3) in §5, $d = 1/\text{AWAR}$ and $D = \text{GRD}$).

An impediment to similar rigorous measurement of GRD for orbital remote sensing systems is the lack of a target of suitable scale on the ground; thus, spatial resolution for most orbiting sensors is described in terms of a less all-encompassing measure, instantaneous field of view (see below). Additional challenges to measuring AWAR for a complete astronaut photography system include the number of different options for aspects of the system including different cameras, films, and orbital altitudes. These elements that must be standardized to determine AWAR provide a useful list of those characteristics of astronaut photography that will most influence GRD.

2.2. *Instantaneous field of view*

The instantaneous field of view (IFOV) is generally used to represent the spatial resolution of automated satellite systems, and is commonly used interchangeably with the term *spatial resolution* when comparing different sensors. IFOV is a combination of geometric, mechanical and electronic properties of the imaging system. Geometric properties including satellite orbital altitude, detector size, and the focal length of the optical system (Simonett 1983). The sensitivity of each detector element at the wavelength desired plus the signal-to-noise level desired are electronic properties that determine a minimum time for energy absorption. For a linear sensor array (pushbroom scanning), this minimum time is translated to areal coverage by the forward velocity of the platform (Campbell 1996, p. 97). Usually, each detector element in the array corresponds to a pixel in the image. Thus for a given altitude, the width of the pixel is determined by the optics and sensor size, and the height of the pixel is determined by the rate of forward motion. When magnified by the ratio of the sensor altitude to the focal length of the optics of the sensor system, IFOV is the size of the area on the ground represented by an individual detector element (pixel, Slater 1980, p. 27).

The equation of IFOV with spatial resolution can be misleading because IFOV does not include factors other than geometry—factors that largely determine the level of detail that can be distinguished in an image. For example, IFOV does not include characteristics of the target (contrast with surroundings, shape of an object, colour), atmospheric conditions, illumination, and characteristics of the interpreter (machine or human). Factors influencing spatial resolution that are included in IFOV can be calculated from design specifications before the system has been built, whereas the actual spatial resolution of an image captured by the sensor will be unique to that image. IFOV represents the best spatial resolution possible given optimal conditions.

2.3. *Imagery from scanners versus film from cameras*

Like aerial photography systems, the GRD of early remote sensing scanners (electro-optical imaging systems), was calibrated empirically (figures 1–6 in Simonett 1983) but such methods are impractical for routine applications. Satellites are now common platforms for collecting remote sensing data, small-scale aerial photographs are widely available within the USA and Europe, and astronaut photographs have become available worldwide. Straightforward comparison of resolutions of photographs to IFOVs of scanner images is necessary for many applications.

How can spatial resolutions of data from different sources be compared using common units? Oft-quoted 'resolution numbers', actually IFOV, of digital scanning systems should be at least doubled for comparison to the standard method of expressing photographic spatial resolution as GRD, simply because of the object contrast requirement. The following rule of thumb has been used in geographic applications to compare spatial resolution of scanners and aerial photography (Welch 1982, Jensen 1983): a low-contrast target may be converted to an approximate IFOV by dividing the GRD (of the photograph) by 2.4. Such a rule of thumb might also be reasonably applied to astronaut photography, making it possible to convert observed GRD to IFOV, and IFOV to an estimated GRD.

In this paper, we discuss the spatial resolution of astronaut photographs in terms of system properties and compute the area on the ground represented by a single pixel, the equivalent to IFOV. To complete our treatment of spatial resolution, we also provide estimates of the sizes of small features identifiable in images, for several cases where this can be readily done.

3. Factors that determine the footprint (area covered by the photograph)

The most fundamental metric that forms the basis for estimating spatial resolution of astronaut photographs is the size of the footprint, or area on the ground captured in a photograph (see review of satellite photogrammetry by Light 1980). The basic geometric variables that influence the area covered by an astronaut photograph are (1) the altitude of the orbit, H, (2) the focal length of the lens, f, (3) the actual size of the image on the film, d, and (4) the orientation of the camera axis relative to the ground (the obliquity or look angle, t). The relationships among these parameters are illustrated in figure 1 (also see equation (3) in §5).

3.1. *Altitude*

Human spaceflight missions have had a variety of primary objectives that required different orbital altitudes. The higher the altitude, the larger the footprint of the photographs. The differing scale of photographs taken at different altitudes is illustrated in figure 2. The two photographs of Lake Eyre, Australia were taken with the same camera and lens, but on different dates and from different altitudes. In (*a*), the lake is relatively flooded, while in (*b*) it is dry. A 2.3 × difference in altitude leads to a corresponding difference in the scales of the resulting photographs.

3.2. *Lenses*

The longer the lens focal length, the more magnification, the greater detail, and the smaller footprint. A variety of lenses with different focal lengths are flown on each space mission (table 1). The effect of lens length on spatial coverage and image detail is shown in figure 3. In these views of Houston (*a*)–(*c*), taken from approximately similar altitudes with the same camera, most of the difference in scale of the

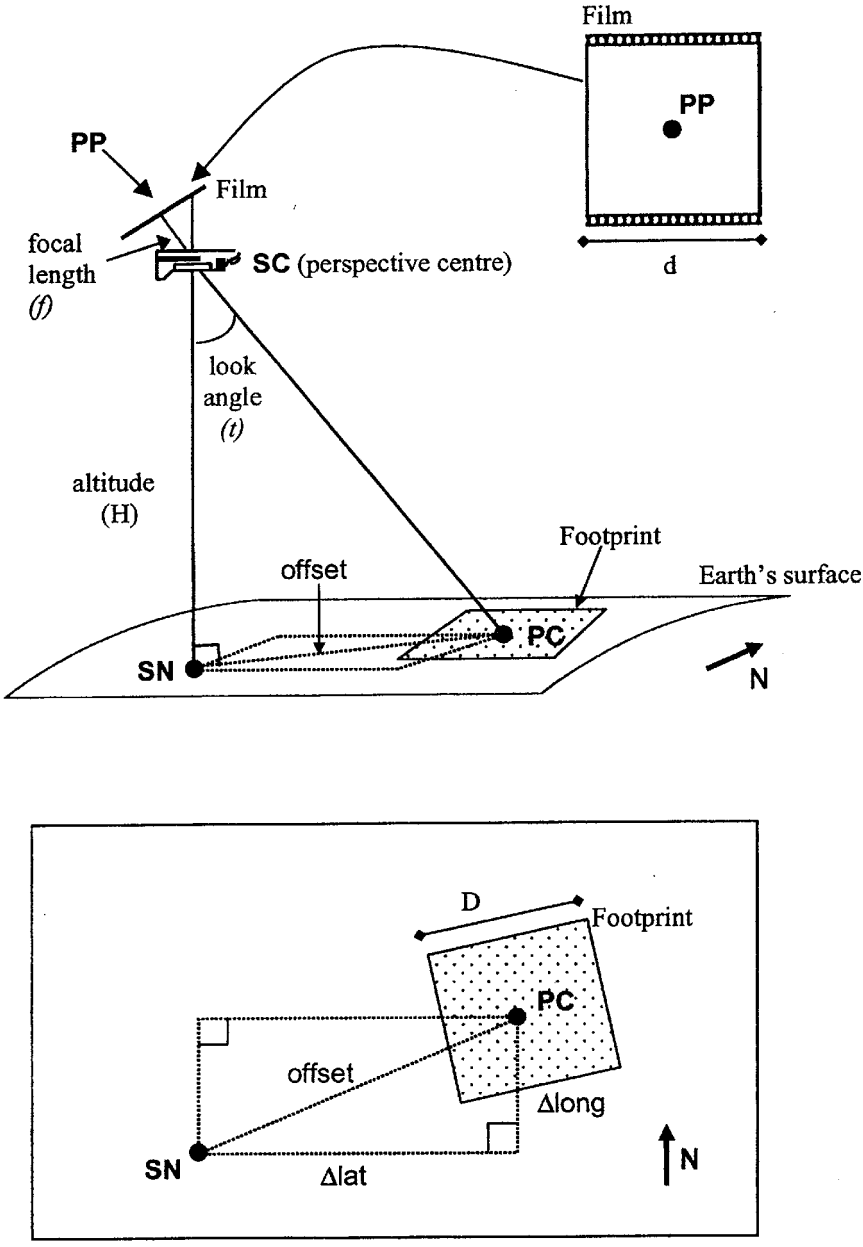

Figure 1. Geometric relationship between look angle (t), spacecraft nadir point (SN), photograph centre point (PC), and photograph principal point (PP). The dark shaded area represents Earth's surface. The distance covered on the ground D corresponds to table 5. Original image size d is listed for various films in table 1. Variables correspond to equations (2)–(9) in §5.

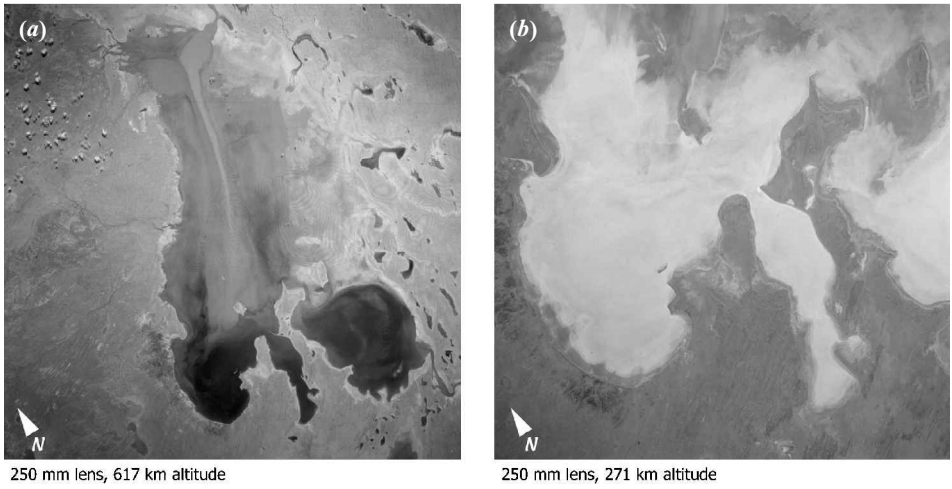

Figure 2. Example of the effect of altitude on area covered in a photograph. Both photographs of Lake Eyre, Australia, were taken using a Hasselblad camera with 100 mm lens: (*a*) altitude 283 km, STS093-702-062; (*b*) altitude 617 km, STS082-754-61.

photographs is due to the different magnifications of the lenses. Although taken from a different altitude and using a different camera with a different original image size (see table 2), an electronic still camera image taken with a 300 mm lens is also included for comparison.

For remote sensing, longer focal length lenses are generally preferred (250 mm or 350 mm for Hasselblad; 300 mm or 400 mm lenses for 35 mm format cameras and ESCs). Unfortunately, longer-focal-length lenses exhibit poorer performance toward the edge of a frame. For example, a 250 mm lens (Distagon CF 5.6) used on the Hasselblad camera has spatial resolution of 57 lp mm^{-1} at the centre, but only 51 lp mm^{-1} at the edge and 46 lp mm^{-1} at the corner (tested with Ektachrome 5017, f/8 aperture and high contrast). A longer 300 mm lens used on the Nikon camera has a greater spatial resolution difference between centre (82 lp mm^{-1}) and corner (49 lp mm^{-1}), using Kodak 5017 Ektachrome, f/4 aperture and high contrast, Fred Pearce (unpublished data). There are tradeoffs among lens optics and speed. For example, the lenses for the Linhof system, and the 250 mm lens for the Hasselblad (Distagon CF 5.6, see footnotes to table 1) are limited to apertures smaller than f/5.6. This becomes an important constraint in selecting shutter speeds (see discussion of shutter speed in §4.2).

3.3. *Cameras and actual image sizes*

After passing through the lens, the photographic image is projected onto film inside the camera. The size of this original image is another important property determining spatial resolution, and is determined by the camera used. Camera formats include 35 mm and 70 mm (Lowman 1980, Amsbury 1989); and occasionally 5×4 inch (127×100 mm) and larger (table 1). Cameras flown on each mission are not metric—they lack vacuum platens or reseau grids, image-motion compensation, or gyro-stabilized mounts. The workhorse for engineering and Earth photography on NASA missions has been a series of 70 mm Hasselblad cameras (table 1), chosen for their reliability. The modified magazine databack imprints a unique number and

Table 1. Details on the cameras used for astronaut photography of Earth. Data include photography from all NASA human spaceflight missions through STS-96 (June 1999, 378 461 total frames in the database)[1].

Camera make	Image size (mm × mm)	Typical lenses used (mm)	Number of photographs	Period of use	Notes
Hasselblad	55 × 55	40, 50, 100, 250[2]	288 494	1963–present	
Linhof	105 × 120	90, 250	29 373	1984–present	Now only flown occasionally
Multispectral Camera (S190A)	57 × 57	152	32 913	1973–1974	Skylab, fixed-mount[3] camera (NASA1974)
Earth Terrain Camera (S190B)	115 × 115	457	5478	1973–1974	Skylab, fixed-mount[3] camera (NASA1974)
Roleiflex	55 × 55	50, 100, 250	4352	1990–1992	
Large Format Camera[4]	229 × 457	305	2143	1984	Mission STS–41G only (Merkel *et al.* 1985)
Maurer	55 × 55	76, 80	818	1961–1968	

[1]Small-format cameras (35 mm film and ESC) are not included in this table because of the large number of lenses and configurations that have been used, and because these data are not currently included in the database for all missions.

[2]Lenses used for Hasselblad manufactured by Carl Zeiss: Distagon CF 4 (40 mm), Distagon CF 4 (50 mm), Distagon CF 3.5 (100 mm), Distagon CF 5.6 (250 mm). Standard Hasselblad lenses flown will change in the year 2000 to Distagon FE 2.8 (50 mm), Distagon FE 2 (110 mm), Tele-Tessar FE 4 (250 mm), and Tele-Tessar FE 4 (350 mm).

[3]These cameras were in fixed mountings on the outside of the Skylab space station. Although not handheld, the film is catalogued with other astronaut photography and is included here for completeness.

[4]A NASA-designed camera with attitude reference system for determining precise nadir points. Data is not currently incorporated into online database, but is cataloged by Merkel *et al.* (1985).

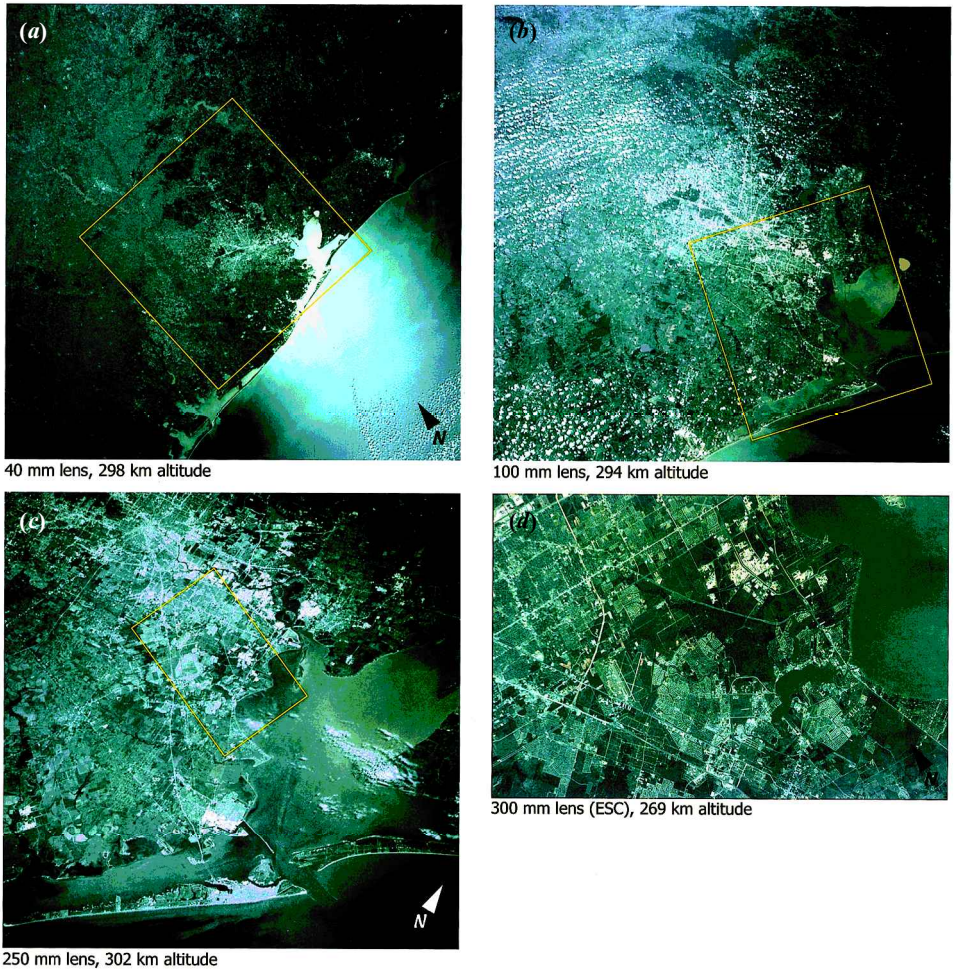

Figure 3. Example of the effect of lens focal length on resolving power. Hasselblad images of Houston were all taken from an altitude of 294 km–302 km with different lenses: (*a*) 40 mm, STS062-97-151; (*b*) 100 mm, STS094-737-28; (*c*) 250 mm STS055-71-41. For comparison, an Electronic Still Camera image with 300 mm lens at 269 km altitude is also shown (*d*) S73E5145.

timestamp on each frame at the time of exposure. Cameras are serviced between flights. Occasionally there is enough volume and mass allowance so that a Linhof 5×4 inch (127×101 mm) format camera can be flown. Nikon 35 mm cameras are flown routinely, also because of proven reliability. Electronic still cameras (ESC) were tested for Earth photography beginning in 1992 (Lulla and Holland 1993). In an ESC, a CCD (charge-coupled device) is used as a digital replacement for film recording the image projected inside the camera. An ESC (consisting of a Kodak DCS 460c CCD in a Nikon N-90S body) was added as routine equipment for handheld photographs in 1995. ESCs have also been operated remotely to capture and downlink Earth images through a NASA-sponsored educational programme (EarthKAM). Discussion of CCD spatial array and radiometric sensitivity are beyond the scope of this paper, but are summarized by Robinson *et al.* (2000b). The

format of the film (or CCD) and image size projected onto the film (or CCD) are summarized for all the different cameras flown in table 2.

3.4. *Look angle or obliquity*

No handheld photographs can be considered perfectly nadir; they are taken at a variety of look angles ranging from near vertical (looking down at approximately the nadir position of the spacecraft) to high oblique (images that include the curvature of Earth). Imaging at oblique look angles leads to an image where scale degrades away from nadir. A set of views of the same area from different look angles is shown in figure 4. The first two shots of the island of Hawaii were taken only a few seconds apart, and with the same lens. The third photograph was taken on a subsequent orbit and with a shorter lens. The curvature of the Earth can be seen in the upper left corner.

Obliquity can be described qualitatively (figure 4) or quantitatively as the look angle (t, figure 1, calculations described in formulation 2 (§5.2)). Because obliquity and look angle have such a dramatic influence on the footprint, we summarize the database characteristics relative to these two parameters. Figure 5 is a breakdown of the spatial resolution characteristics of low oblique and near vertical photographs in the NASA Astronaut Photography database. Number of photographs are grouped (1) by calculated values for look angle (t) and (2) by altitude. After observing the overlap between near vertical and low oblique classes, we are currently restructuring this variable ('tilt') in the database to provide a measure of t when available. Users will still be able to do searches based on the qualitative measures, but these measures will be more closely tied to actual look angle.

3.4.1. *Obliquity and georeferencing digitised photographs*

Often the first step in a remote sensing analysis of a digitized astronaut photograph is to georeference the data and resample it to conform to a known map projection. Details and recommendations for resampling astronaut photography data are provided by Robinson *et al.* (2000a, 2000c) and a tutorial is also available (McRay *et al.* 2000). Slightly oblique photographs can be geometrically corrected for remote sensing purposes, but extremely oblique photographs are not suited for geometric correction. When obliquity is too great, the spatial scale far away from nadir is much larger than the spatial scale closer to nadir; resampling results are unsuitable because pixels near nadir are lost as the image is resampled while many pixels far away from nadir are excessively replicated by resampling.

To avoid the generation of excess pixels during georeferencing, the pixel sizes of the original digitized image should be smaller than the pixels in the final resampled image. Calculations of original pixel size using methods presented below can be useful in ensuring meaningful resampling. For slightly oblique images, formulation 3 (§5.3) can be used to estimate pixel sizes at various locations in a photograph (near nadir and away from nadir), and these pixel sizes then used to determine a reasonable pixel scale following resampling.

4. Other characteristics that influence spatial resolution

Beyond basic geometry, many other factors internal to the astronaut photography system impact the observed ground resolved distance in a photograph. The lenses and cameras already discussed are imperfect and introduce radiometric degradations (Moik 1980).Vignetting (slight darkening around the edges of an image) occurs in

Table 2. Maximum possible digital spatial resolution (pixel size in m) for camera systems currently used by astronauts to photograph earth, based on the geometry of altitude, lens, and film size. Calculations assume that colour transparency film is digitized at 2400 ppi (pixels per inch, 10.6 μm pixel^{-1}).

Camera system		Image size		Minimum ground distance represented by 1 pixel (m) As a function of altitude[1]		
		mm × mm	pixels[2]	Minimum altitude (222 km)	Median altitude (326 km)	Maximum altitude (611 km)
Linhof 125 mm	90 mm lens	105 × 120	8978 × 11 434	26.1	38.3	71.8
	250 mm lens			9.4	13.8	25.9
Hasselblad 70 mm	100 mm lens	55 × 55	5198 × 5198	23.5	34.5	64.7
	250 mm lens			9.4	13.8	25.9
Nikon 35 mm	300 mm lens	36 × 24	3308 × 2174	7.8	11.5	21.6
	400 mm lens			5.9	8.6	16.2
ESC 35 mm	180 mm lens[3]	27.6 × 18.5	3069 × 2043	11.1	16.3	30.6
	300 mm lens			6.7	9.8	18.4
	400 mm lens			5.0	7.4	13.8

[1]Altitudes shown are minimum, median and maximum through STS-89 (January 1998, $N = 84$ missions).
[2]Actual pixels for ESC, otherwise assumed digitization at 2400 ppi (pixels per inch), equal to 10.6 μm pixel^{-1}.
[3]The most common configuration for Earth photography as part of the EarthKAM project.

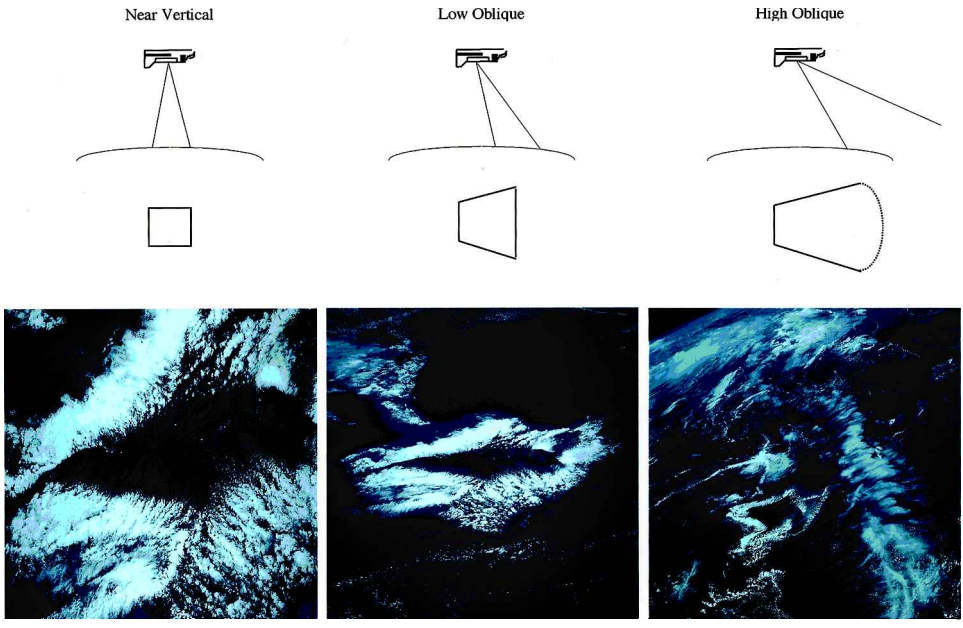

Figure 4. Definitions of look angle for photographs taken from low orbit around Earth. The example photographs of Hawaii were all taken from approximately the same altitude (370–398 km) and with the same (250 mm) lens on a Hasselblad camera (STS069-701-69, STS069-701-70, and STS069-729-27 [100 mm lens]).

astronaut photography due to light path properties of the lenses used. A lack of flatness of the film at the moment of exposure (because cameras used in orbit do not incorporate a vacuum platen) also introduces slight degradations. A number of additional sources of image degradation that would affect GRD of astronaut photographs are listed.

4.1. *Films and processing*

4.1.1. *Colour reversal films*

Most films used in NASA handheld cameras in orbit have been E-6 process colour reversal films (Ektachromes) that have a nominal speed of 64 to 100 ASA, although many other films have been flown (table 3). Reversal films are used because damage from radiation exposure while outside the atmospheric protection of Earth is more noticeable in negative films than in positive films (Slater 1996). The choice of ASA has been to balance the coarser grains (lower film resolving power) of high-speed films with the fact that slower films require longer exposures and thus are affected more by vehicle motion (approximately 7.3 km s^{-1} relative to Earth's surface for the Space Shuttle). Extremely fast films (>400 ASA) are also more susceptible to radiation damage in orbit (particularly during long-duration or high-altitude missions, Slater 1996) and have not traditionally been used for Earth photography. The manufacturer stock numbers identifying the film used are available for each image in the Astronaut Photography Database (Office of Earth Sciences 2000).

4.1.2. *Colour infrared films*

Colour infrared film (CIR) was used during an Earth-orbiting Apollo mission (Colwell 1971), in the multispectral S-190A and the high-resolution S-190B camera

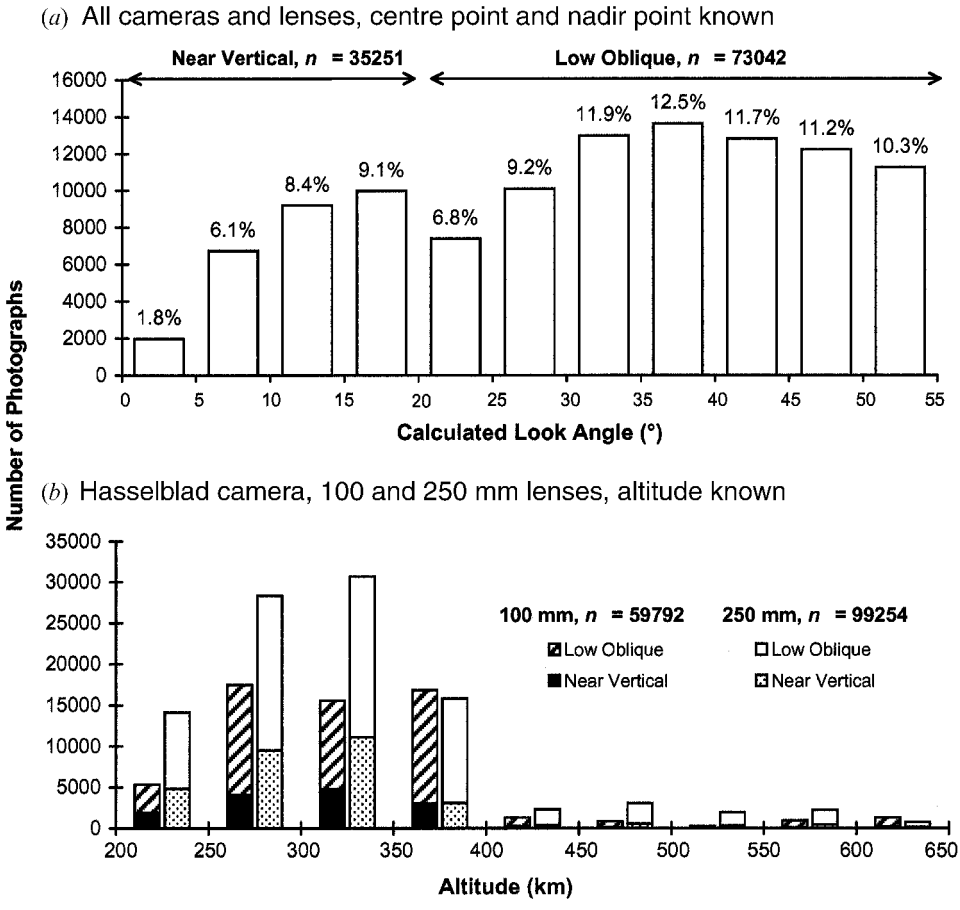

Figure 5. (*a*) Distributions of astronaut photographs by look angle off-nadir (calculated from centre point and nadir point using Formulation 2). Data included for all photographs for which centre and nadir points are known, with high oblique look angles ($n=$ 55 155) excluded. (Total sample shown is 108 293 of 382 563 total records in the database when compiled. For records where nadir data was not available, number of observations for qualitative look angles are: near vertical, 14 086; low oblique, 115 834; undetermined, 89 195.) (*b*) Altitude distribution for astronaut photographs of Earth taken with the Hasselblad camera. Data included for Hasselblad camera only, focal length determined, with high oblique look angles excluded. (Total sample shown is 159 046 of 206 971 Hasselblad records with known altitude and of 382 563 total records in the database when compiled. For Hasselblad records with known altitude, data not shown includes high oblique photographs using 100 mm and 250 mm lenses, $n=20\,262$, and all look angles with other lenses, $n=27\,663$.)

systems on Skylab (NASA 1974, Wilmarth *et al.* 1977), and occasionally on Shuttle missions and Shuttle-*Mir* missions (table 3). The CIR film used is a three-layer Aerochrome, having one layer that is sensitive to reflected solar infrared energy to approximately 900 nm (Eastman Kodak Company 1998); protective coatings on most spacecraft windows also limit IR transmittance between 800 mm and 1000 nm. This layer is extremely sensitive to the temperature of the film, which creates unpredictable degradation of the IR signature under some spaceflight conditions.

Table 3. Details on films used for astronaut photography of Earth. Data include photography from all NASA human spaceflight missions through STS-96 (June 1999; 378 461 total frames in the database). Films with < 5000 frames exposed and films used for 35 mm cameras only are not included.

Film manufacturer	ASA	Resolving power[1]	Number of frames	Period of use	Cameras
Colour positive					
Kodak Aerochrome II (2447, 2448, SO-131, SO-368)	32	40–50	5138	1968–1985	Hasselblad, Linhof
Kodak Ektachrome (5017, 5025, 6017, 6118, SO-121, SO-217, QX-824, QX-868)	64	50	113 932	1965–1968, 1981–1993	Hasselblad, Linhof, Roleiflex, Maurer, Nikon
Kodak Lumiere (5046, 5048)	100		105 743	1994–1998	Hasselblad, Linhof
Kodak Elite 100S (5069)	100		41 486	1996–present	Hasselblad[2]
Fuji Velvia 50, CS 135-36	32		13 882	1992–1997	Hasselblad, Nikon
Kodak Hi-Resolution Color (SO-242, SO-356)		100	9674	1973–1975	Hasselblad, S190A, S190B
Infrared and black-and-white films					
Kodak Aerochrome Color Infrared (8443, 3443, 2443)	40	32	40 704	1965–present[2]	Hasselblad, Linhof, Nikon, S190A, S190B
Kodak B&W Infrared (2424)		32	10 553	1973–1974	S190A
Kodak Panatomic-X B&W (SO-022)		63	10 657	1973–1974	S190A

[1] At low contrast (object/background ratio 1.6/1), as provided by Kodak and listed by Slater *et al.* (1983:256). Resolving power was discontinued from the technical tests performed by Kodak in approximately 1993, and it is not known if current films have similar resolving power to older versions of similar films (K. Teitelbaum, Kodak, personal communication). The granularity measure now provided by Kodak cannot be readily converted to a spatial resolution.

[2] The Linhof was used again on STS-103 in December 1999 (data not catalogued as of the preparation of this table) using Kodak Elite 100S film.

[3] Beginning in July 1999, 2443 colour-infrared film process was changed from EA-5 to E-6.

4.1.3. *Film duplication*

The original film is archived permanently after producing about 20 duplicate printing masters (second generation). Duplicate printing masters are disseminated to regional archives and used to produce products (third–fourth generation) for the media, the public, and for scientific use. When prints, slides, transparencies, and digital products are produced for public distribution, they are often colour adjusted to correspond to a more realistic look. Digital products from second generation copies can be requested by scientific users (contact the authors for information on obtaining such products for a particular project), and these are recommended for remote sensing applications. Care should be taken that the digital product acquired for remote sensing analysis has not been colour adjusted for presentation purposes. Based on qualitative observations, there is little visible increase in GRD in the third or fourth generation products. There is a significant degradation in fidelity of colour in third and fourth generation duplicates, because an increase in contrast occurs with every copy.

4.2. *Shutter speeds*

The impact of camera motion (both due to the photographer and to the motion of the spacecraft) on image quality is determined by shutter speed—1/250 to 1/500 second have been used, because slower speeds record obvious blurring caused by the rapid motion of the spacecraft relative to the surface of the Earth. Generally 1/250 was used for ISO 64 films (and slower), and after the switch to ISO 100 films, a 1/500 setting became standard. New Hasselblad cameras that have been flown beginning with STS-92 in October 2000 vary shutter speed using a focal plane shutter for exposure bracketing (rather than varying aperture) and 1/250, 1/500 and 1/1000 second are used.

Across an altitude range of 120–300 nautical miles (222–555 km) and orbital inclinations of 28.5° and 57.0°, the median relative ground velocity of orbiting spacecraft is 7.3 km s^{-1}. At a nominal shutter speed of 1/500, the expected blur due to motion relative to the ground would be 14.6 m. When cameras are handheld (as opposed to mounted in a bracket), blur can be reduced by physical compensation for the motion (tracking) by the photographer; many photographs show a level of detail indicating that blur at this level did not occur (e.g. figure 3(*d*)). Thus, motion relative to the ground is not an absolute barrier to ground resolution for handheld photographs.

4.3. *Spacecraft windows*

Most of the photographs in the NASA Astronaut Photography Database were taken through window ports on the spacecraft used. The transmittance of the window port may be affected by material inhomogeniety of the glass, the number of layers of panes, coatings used, the quality of the surface polish, environmentally induced changes in window materials (pressure loads, thermal gradients), or deposited contamination. Such degradation of the window cannot be corrected, is different for each window, and changes over time. See Eppler *et al*. (1996) and Scott (2000) for discussion of the spectral transmittance of the fused quartz window that is part of the US Laboratory Module (*Destiny*) of the International Space Station.

4.4. *Digitized images from film*

When film is scanned digitally the amount of information retained depends on the spectral information extracted from the film at the spatial limits of the scanner.

To date, standard digitizing methodologies for astronaut photographs have not been established and film is digitized on a case-by-case basis using the equipment available.

4.4.1. *Digitizing and spatial resolution*

Light (1993, 1996) provided equations for determining the digitizing spatial resolution needed to preserve spatial resolution of aerial photography based on the static resolving power (AWAR) for the system. For films where the manufacturer has provided data (Eastman Kodak 1998, K. Teitelbaum, personal communication), the resolving power of films used for astronaut photography ranges from 32 lp mm^{-1} to 100 lp mm^{-1} at low contrast (object/background ratio 1.6/1, table 3). The AWAR for the static case of the Hasselblad camera has been measured at high and low contrast (using lenses shown in table 1), with a maximum of approximately 55 lp mm^{-1} (Fred Pearce, unpublished data).

Based on the method of Light (1993, 1996), the dimension of one spatial resolution element for a photograph with maximum static AWAR of 55 lp mm^{-1} would be 18 μm lp^{-1}. The acceptable range of spot size to preserve spatial information would then be

$$\frac{18\ \mu\text{m}}{2\sqrt{2}} \leqslant \text{scan spot size} \leqslant \frac{18\ \mu\text{m}}{2} \tag{1}$$

and 6 μm $\leqslant$ scan spot size $\leqslant$ 9 μm. Similarly, for a more typical static AWAR of 30 lp mm^{-1} (33 μm lp^{-1}, low contrast, Fred Pearce, unpublished data) 11 μm $\leqslant$ scan spot size $\leqslant$ 17 μm. These scan spot sizes correspond to digitizing resolutions ranging from 4233–2822 ppi (pixels inch^{-1}) for AWAR of 55 lp mm^{-1} and 2309–1494 ppi for AWAR of 30 lp mm^{-1}. Scan spot sizes calculated for astronaut photography are comparable to those calculated for the National Aerial Photography Program (9–13 μm, Light 1996).

Widely available scanners that can digitize colour transparency film currently have a maximum spatial resolution of approximately 2400 ppi (10.6 μm pixel^{-1}). For example, we routinely use an Agfa Arcus II desktop scanner (see also Baltsavias 1996) with 2400 ppi digitizing spatial resolution (2400 ppi optical resolution in one direction, and 1200 ppi interpolated to 2400 ppi in the other direction) and 2400 ppi was used to calculate IFOV equivalents (tables 2 and 4). For some combinations of lens, camera, and contrast, 2400 ppi will capture nearly all of the spatial information contained in the film. However, for film with higher resolving power than Ektachrome-64, for better lenses, and for higher contrast targets, digitizing at 2400 ppi will not capture all of the spatial information in the film.

Improvements in digitizing technology will only produce real increases in IFOV to the limit of the AWAR of the photography system. The incremental increase in spatial information above 3000 ppi (8.5 μm pixel^{-1}) is not likely to outweigh the costs of storing large images (Luman *et al.* 1997). At 2400 ppi, a Hasselblad frame is approximately 5200 $\times$ 5200 or 27 million pixels (table 2) while the same image digitized at 4000 ppi would contain 75 million pixels.

Initial studies using astronaut photographs digitized at 2400 ppi (10.6 μm pixel^{-1}, Webb *et al.* 2000, Robinson *et al.* 2000c) indicate that some GRD is lost compared to photographic products. Nevertheless, the spatial resolution is still comparable with other widely used data sources (Webb *et al.* 2000). Robinson *et al.* (2000c) found that digitizing at 21 μm pixel^{-1} provided information equivalent to 10.6 μm pixel^{-1} for identifying general urban area boundaries for six cities, except for a single

photo that required higher spatial resolution digitizing (it had been taken with a shorter lens and thus had less spatial resolution). Part of the equivalence observed in the urban areas study may be attributable to the fact that the flatbed scanner used interpolates from 1200 ppi to 2400 ppi in one direction. The appropriate digitizing spatial resolution will, in part, depend on the scale of features of interest to the researchers, with a maximum upper limit set of a scan spot size of approximately 6 μm (4233 ppi).

4.4.2. *Digitizing and spectral resolution*

When colour film is digitized, there will be loss of spectral resolution. The three film emulsion layers (red, green, blue) have relatively distinct spectral responses, but are fused together so that digitizers detect one colour signal and must convert it back into three (red, green, blue) digital channels. Digital scanning is also subject to spectral calibration and reproduction errors. Studies using digital astronaut photographs to date have used 8 bits per channel. However, this is another parameter that can be controlled when the film is digitized. We do not further address spectral resolution of digitally scanned images in this paper.

4.5. *External factors that influence GRD*

Although not discussed in detail in this paper, factors external to the spacecraft and camera system (as listed by Moik (1980) for remote sensing in general) also impact GRD. These include atmospheric interference (due to scattering, attenuation, haze), variable surface illumination (differences in terrain slope and orientation), and change of terrain reflectance with viewing angle (bidirectional reflectance). For astronaut photographs, variable illumination is particularly important because orbits are not sun-synchronous. Photographs are illuminated by different sun angles and images of a given location will have colour intensities that vary widely. In addition, the viewing angle has an effect on the degree of object-to-background contrast and atmospheric interference.

5. Estimating spatial resolution of astronaut photographs

In order to use astronaut photographs for digital remote sensing, it is important to be able to calculate the equivalent to an IFOV—the ground area represented by a single pixel in a digitized orbital photograph. The obliquity of most photographs means that pixel 'sizes' vary at different places in an image. Given a ground distance, D represented by a photograph in each direction (horizontal, vertical) an approximate average pixel width (P, the equivalent of IFOV) for the entire image can be calculated as follows:

$$P = \frac{D}{dS} \tag{2}$$

where D is the projected distance on the ground covered by the image in the same direction as the pixel is measured, d is the actual width of the image on the original film (table 1), and S is the digitizing spatial resolution.

Here, we present three mathematical formulations for estimating the size of the footprint, or area on the ground covered by the image. Example results from the application of all three formulations are given in table 5. The first and simplest calculation (formulation 1) gives an idea of the maximum spatial resolution attainable at a given altitude of orbit with a given film format and a perfectly vertical (nadir)

view downward. Formulation 2 takes into account obliquity by calculating look angle from the difference between the location on the ground represented at the centre of the photograph, and the nadir location of the spacecraft at the time the photograph was taken (figure 1). Formulation 3 describes an alternate solution to the oblique look angle problem using coordinate-system transformations. This formulation has been implemented in a documented spreadsheet and is available for download (http://eol.jsc.nasa.gov/SearchPhotos/Low_Oblique_301_Locked.xls), and is in the process of being implemented on a Web-based user interface to the Astronaut Photography Database (Office of Earth Sciences 2000).

Although formulations 2 and 3 account for obliquity, for the purposes of calculation they treat the position of the spacecraft and position of the camera as one. In actuality, astronauts are generally holding the cameras by hand (although cameras bracketed in the window are also used), and the selection of window, position of the astronaut in the window, and rotation of the camera relative to the movement of the spacecraft are not known. Thus, calculations using only the photo centre point (PC) and spacecraft nadir point (SN) give a *locator ellipse* and not the locations of the corners of the photograph. A locator ellipse describes an estimated area on the ground that is likely to be included in a specific photograph regardless of the rotation of the film plane about the camera's optical axis (figure 6).

Estimating the corner positions of the photo requires additional user input of a single auxiliary point—a location on the image that has a known location on the ground. Addition of this auxiliary point is an option available to users of the spreadsheet. An example of the results of adding an auxiliary point is shown in figure 7 with comparisons of the various calculations in table 5.

5.1. *Formulation 1. Footprint for a nadir view*

The simplest way to estimate footprint size is to use the geometry of camera lens and spacecraft altitude to calculate the scaling relationship between the image in the

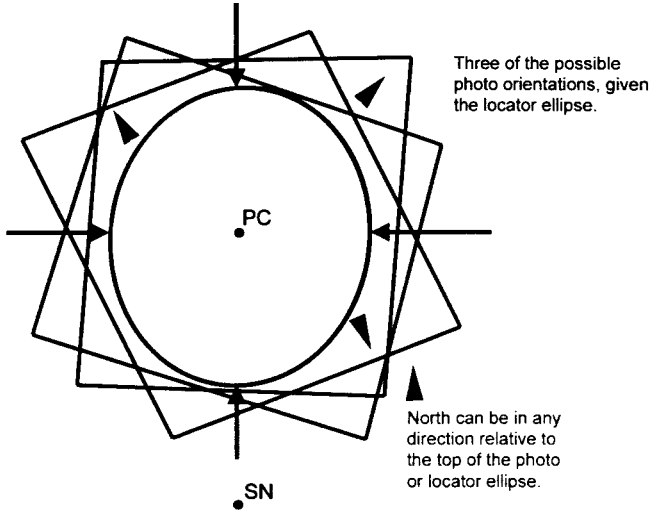

Figure 6. Sketch representation of the locator ellipse, an estimated area on the ground that is likely to be included in a specific photograph regardless of the rotation of the film plane about the camera's optical axis.

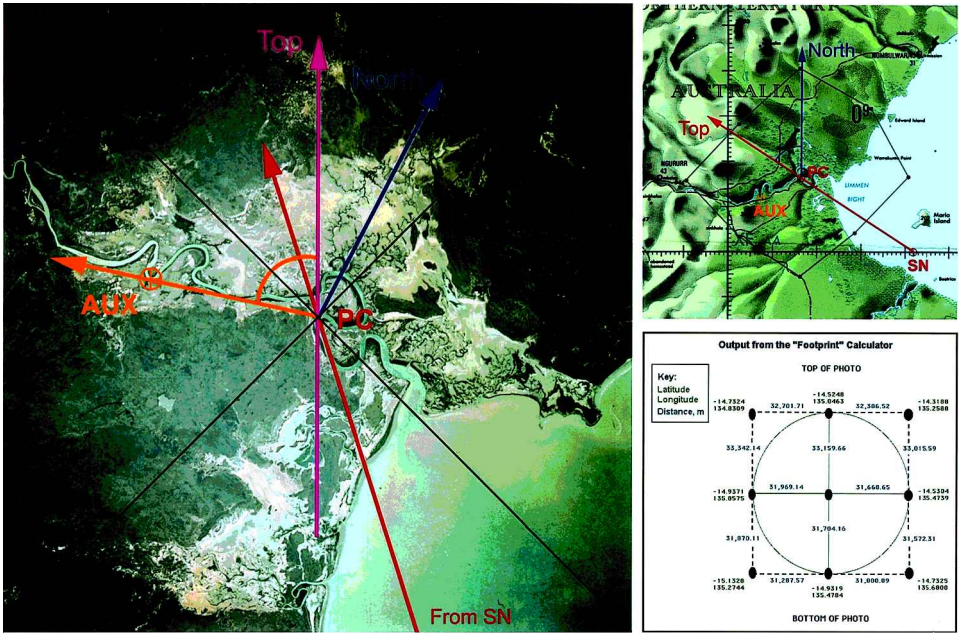

Figure 7. An example of the application of the Low Oblique Space Photo Footprint Calculator. The photograph (STS093-704-50) of Limmen Bight, Australia, was taken from an altitude of 283 km using the Hasselblad camera with a 250 mm lens. Map used is 1:1 000 000 Operational Navigational Chart. The distances shown equate to an average pixel size of 12.4 m for this photograph.

film and the area covered on the ground. For a perfect nadir view, the scale relationship from the geometry of similar triangles is

$$\frac{d}{D} = \frac{f}{H} \tag{3}$$

where d = original image size, D = distance of footprint on the ground, f = focal length of lens, and H = altitude. Once D is known, pixel size (length = width) can be calculated from equation (2). These calculations represent the minimum footprint and minimum pixel size possible for a given camera system, altitude and digitising spatial resolution (table 2). Formulation 1 was used for calculating minimum pixel sizes shown in tables 2 and 4.

By assuming digitizing at 2400 ppi (10.6 μm pixel^{-1}), currently a spatial resolution commonly attainable from multipurpose colour transparency scanners (see §4.4.1), this formulation was used to convert area covered to an IFOV equivalent for missions of different altitudes (table 2). Table 4 provides a comparison of IFOV of images from various satellites, including the equivalent for astronaut photography. Values in this table were derived by using formulation 1 to estimate the area covered because a perfect nadir view represents the best possible spatial resolution and smallest field of view that could be obtained.

5.2. *Formulation 2. Footprint for oblique views using simplified geometry and the great circle distance*

A more realistic approach to determining the footprint of the photograph accounts for the fact that the camera is not usually pointing perfectly down at the

Table 4. Comparison of pixel sizes (instantaneous fields of view) for satellite remote sensors with pixel sizes for near vertical viewing photography from spacecraft. Note that all data returned from the automated satellites have the same field of view, while indicated pixel sizes for astronaut photography are best-case for near vertical look angles. See figure 5 for distributions of astronaut photographs of various look angles. High-altitude aerial photography is also included for reference.

Instrument	Altitude (km)	Pixel width (m × m)	Bands[1]
Landsat Multipectral Scanner[2] (MSS, 1974-)	880–940	79 × 56	4–5
Landsat Thematic Mapper (TM, 1982-)	~705	30 × 30	7
Satellite pour l'Observation de la Terre (SPOT, 1986-)	~832		
SPOT 1-3 Panchromatic		10 × 10	1
SPOT 1-3 Multispectral (XS)		20 × 20	3
Astronaut Photography (1961-)			
Skylab[3] (1973-1974)	~435		
Multispectral Camera (6 camera stations)		17–19 × 17–19	3–8
Earth Terrain Camera (hi-res colour)		8.75 × 8.75	3
Space Shuttle[5] (1981-)	222–611		
Hasselblad 70 mm (250mm lens, colour), vertical view		9–26 × 9–26	3
Hasselblad 70 mm (100mm lens, colour), vertical view		23–65 × 23–65	3
Nikon 35 mm (400mm lens, colour film or ESC), vertical		5–16 × 5–16	3
High Altitude Aerial Photograph (1:100 000)	~1.2	2 × 2	3

[1]Three bands listed for aerial photography obtainable by high-resolution colour digitizing. For high-resolution colour film at 65 lp mm^{-1} (K. Teitelbaum, Eastman Kodak Co., personal communication) the maximum information contained would be 3302 ppi.

[2]Data from Simonett (1983:Table 1-2).

[3]Calculated as recommended by Jensen (1983:1596): the dividend of estimated ground resolution at low contrast given in NASA (1974:179-180) and 2.4.

[4]Six filters plus colour and colour infrared film (NASA 1974:7).

[5]Extracted from table 2.

nadir point. The look angle (the angle off nadir that the camera is pointing) can be calculated trigonometrically by assuming a spherical earth and calculating the distance between the coordinates of SN and PC (figure 1) using the Great Circle distance, haversine solution (Sinnott 1984, Snyder 1987:30–32, Chamberlain 1996). The difference between the spacecraft centre and nadir point latitudes, $\Delta lat = lat\,2 - lat\,1$, and the difference between the spacecraft centre and nadir point longitudes, $\Delta lon = lon\,2 - lon\,1$, enter the following equations:

$$a = \sin^2\left(\frac{\Delta lat}{2}\right) + \cos(lat\,1)\cos(lat\,2)\sin^2\left(\frac{\Delta lon}{2}\right) \tag{4}$$

$$c = 2\arcsin(\min[1, \sqrt{a}]) \tag{5}$$

and $offset = R\,c$, with R the radius of a spherical Earth = 6370 km.

The look angle (t) is then given by

$$t = \arctan\left(\frac{offset}{H}\right) \tag{6}$$

Assuming that the camera was positioned so that the imaginary line between the centre and nadir points (the principal line) runs vertically through the centre of the photograph, the distance between the geometric centre of the photograph (principal point, PP) and the top of the photograph is $d/2$ (figure 8(a)). The scale at any point

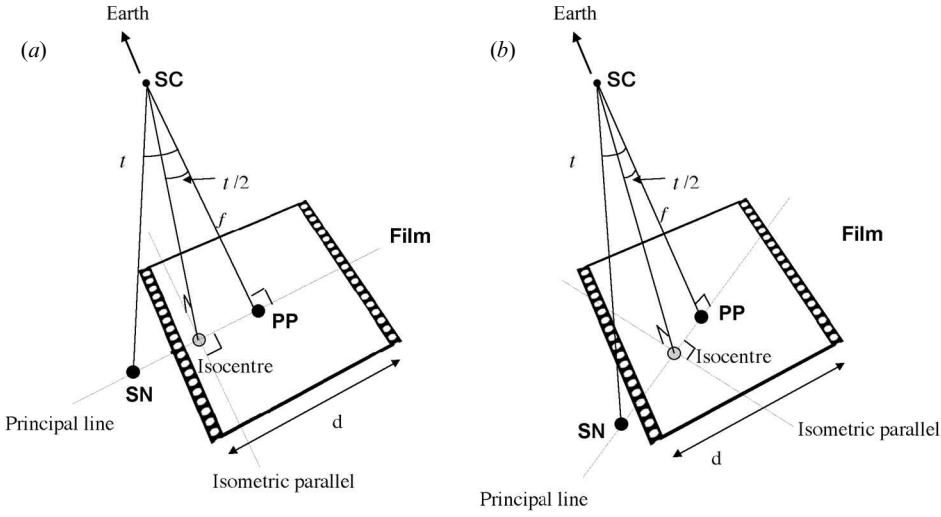

Figure 8. The geometric relationship between look angle, lens focal length and the centre point and nadir points of a photograph (see also Estes and Simonett 1975). Note that the Earth's surface and footprint represented in figure 1 are not shown here, only a representation of the image area of the photograph. Variables shown in the figure: look angle, t; focal length, f; *PP*, centre of the image on the film; *SN*, spacecraft nadir; d, original image size. (*a*) The special case where the camera is aligned squarely with the isometric parallel. In this case, tilt occurs along a plane parallel with the centre of the photograph. When the conditions are met, calculations using Formulation 3 will give the ground coordinates of the corner points of the photograph. (*b*) The general relationship between these parameters and key photogrammetric points on the photograph. For this more typical case, coordinates of an additional point in the photograph must be input in order to adjust for twist of the camera and to find the corner point coordinates.

in the photograph varies as a function of the distance, y, along the principal line between the isocentre and the point according to the relationship

$$\frac{d}{D}=\frac{f-y\sin t}{H} \tag{7}$$

(Wong 1980, equation (2.14), $H \gg$ the ground elevation, h). Using figure 8(*a*) at the top of the photo,

$$y=f\tan\left(\frac{t}{2}\right)+\frac{d}{2} \tag{8}$$

and at the bottom of the photo,

$$y=f\tan\left(\frac{t}{2}\right)-\frac{d}{2} \tag{9}$$

Thus, for given PC and SN coordinates and assuming a photo orientation as in figure 8(*a*) and not figure 8(*b*), we can estimate a minimum D (using equations (7) and (8)) and a maximum D (using equations (7) and (9)), and then average the two to determine the pixel size (P) via equation (2).

5.3. *Formulation 3. The Low Oblique Space Photo Footprint Calculator*

The Low Oblique Space Photo Footprint Calculator was developed to provide a more accurate estimation of the geographic coordinates for the footprint of a low oblique photo of the Earth's surface taken from a human-occupied spacecraft in orbit. The calculator performs a series of three-dimensional coordinate transformations to compute the location and orientation of the centre of the photo exposure plane relative to an earth referenced coordinate system. The nominal camera focal length is then used to create a vector from the photo's perspective point, through each of eight points around the parameter of the image, as defined by the format size. The geographical coordinates for the photo footprint are then computed by intersecting these photo vectors with a spherical earth model. Although more sophisticated projection algorithms are available, no significant increase in the accuracy of the results would be produced by these algorithms due to inherent uncertainties in the available input data (i.e. the spacecraft altitude, photo centre location, etc.).

The calculations were initially implemented within a Microsoft Excel workbook, which allowed one to embed the mathematical and graphical documentation next to the actual calculations. Thus, interested users can inspect the mathematical processing. A set of error traps was also built into the calculations to detect erroneous results. A summary of any errors generated is reported to the user with the results of the calculations. Interested individuals are invited to download the Excel workbook from http://eol.jsc.nasa.gov/SearchPhotos/Low_Oblique_301_Locked.xls . The calculations are currently being encoded in a high-level programming language and should soon be available alongside other background data provided for each photograph at Office of Earth Sciences (2000).

For the purposes of these calculations, a low oblique photograph was defined as one with the centre within 10 degrees of latitude and longitude of the spacecraft nadir point. For the typical range of spacecraft altitudes to date, this restricted the calculations to photographs in which Earth's horizon does not appear (the general definition of a low oblique photograph, e.g. Campbell 1996:71, and figure 4).

5.3.1. *Input data and results*

Upon opening the Excel workbook, the user is presented with a program introduction providing instructions for using the calculator. The second worksheet tab 'How-To-Use', provides detailed step-by-step instructions for preparing the baseline data for the program. The third tab 'Input-Output' contains the user input fields and displays the results of the calculations. The additional worksheets contain the actual calculations and program documentation. Although users are welcome to review these sheets, an experienced user need only access the 'Input-Output' spreadsheet.

To begin a calculation the user enters the following information which is available for each photo in the NASA Astronaut Photography Database: (1) SN, geographical coordinates of spacecraft nadir position at the time of photo; (2) H, spacecraft altitude; (3) PC, the geographical coordinates of the centre of the photo; (4) f, nominal focal length; and (5) d, image format size. The automatic implementation of the workbook on the web will automatically enter these values and complete calculations.

For more accurate results the user may optionally enter the geographic coordinates and orientation for an auxiliary point on the photo, which resolves the camera's rotation uncertainty about the optical axis. The auxiliary point data must

be computed by the user following the instruction contained in the 'How-To-Use' tab of the spreadsheet.

After entering the input data the geographic coordinates of the photo footprint (i.e. four photo corner points, four points at the bisector of each edge and the centre of the photo) are immediately displayed below the input fields along with any error messages generated by the user input or by the calculations (figure 7). Although results are computed and displayed, they should not be used when error messages are produced by the program. The program also computes the tilt angle for each of the photo vectors relative to the spacecraft nadir vector. To the right of the photo footprint coordinates is displayed the arc distance along the surface of the sphere between adjacent computed points.

5.3.2. *Calculation assumptions*

The mathematical calculations implemented in the Low Oblique Space Photo Footprint Calculator use the following assumptions:

1. The *SN* location is used as exact, even though the true value may vary by up to ± 0.1 degree from the location provided with the photo.
2. The spacecraft altitude is used as exact. Although the determination of the nadir point at the instant of a known spacecraft vector is relatively precise ($\pm 1.15 \times 10^{-4}$ degrees), the propagator interpolates between sets of approximately 10–40 known vectors per day, and the time code recorded on the film can drift. Thus, the true value for *SN* may vary by up to ± 0.1 degree from the value provided with the photo.
3. The perspective centre of the camera is assumed to be at the given altitude over the specified spacecraft nadir location at the time of photo exposure.
4. The *PC* location is used as exact, even though the true value may vary by up to $\pm 0.5^{\circ}$ latitude and $\pm 0.5^{\circ}$ longitude from the location provided with the photo.
5. A spherical earth model is used with a nominal radius of 6 372 161.54 m (a common first-order approximation for a spherical earth used in geodetic computations).
6. The nominal lens focal length of the camera lens is used in the computations (calibrated focal length values are not available).
7. The photo projection is based on the classic pin-hole camera model.
8. No correction for lens distortion or atmospheric reflection is made.
9. If no auxiliary point data is provided, the 'Top of the Image' is oriented perpendicular to the vector from *SN* towards *PC*.

5.3.3. *Transformation from Earth to photo coordinate systems*

The calculations begin by converting the geographic coordinates (latitude and longitude) of the *SN* and *PC* to a Rectangular Earth-Centred Coordinate System (R-Earth), defined as shown in figure 9 (with the centre of the Earth at (0, 0, 0)). Using the vector from the Earth's centre through SN and the spacecraft altitude, the spacecraft location (*SC*) is also computed in R-Earth.

For ease of computation, a Rectangular Spacecraft-Centred Coordinate System (R-Spacecraft) is defined as shown in figure 9. The origin of R-Spacecraft is located at *SC*, with its $+Z$-axis aligned with vector from the centre of the Earth through *SN* and its $+X$-axis aligned with the vector from *SN* to *PC* (figure 9). The specific

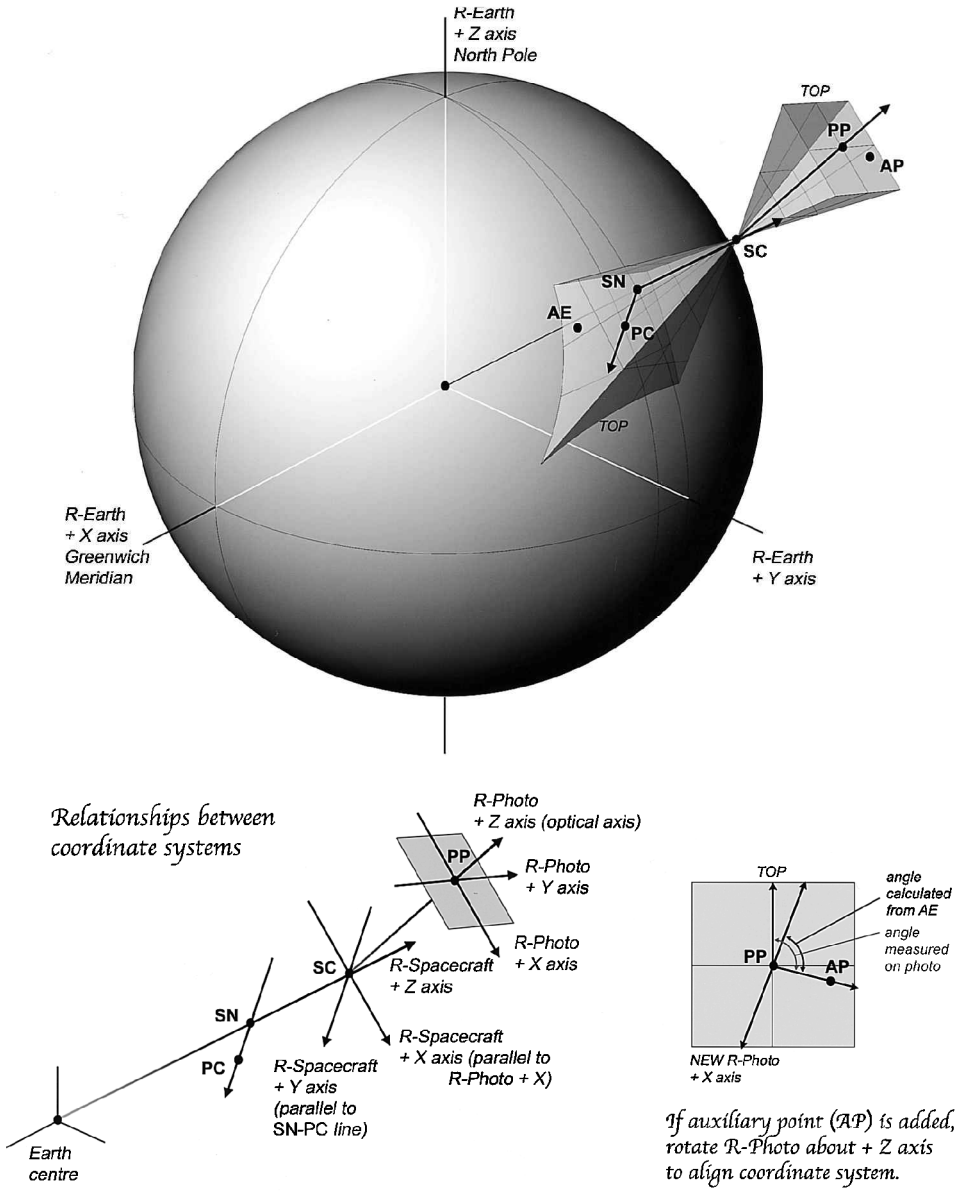

Figure 9. Representation of the area included in a photograph as a geometric projection onto the Earth's surface. Note that the focal length (the distance from the Space Shuttle to the photo) is grossly overscale compared to the altitude (the distance from the Shuttle to the surface of the Earth.

rotations and translation used to convert from the R-Earth to the R-Spacecraft are computed and documented in the spreadsheet.

With the mathematical positions of the *SC*, *SN*, *PC*, and the centre of the Earth computed in R-Spacecraft, the program next computes the location of the camera's principal point (*PP*). The principle point is the point of intersection of the optical axis of the lens with the image plane (i.e. the film). It is nominally positioned at a

distance equal to the focal length from the perspective centre of the camera (which is assumed to be at *SC*) along the vector from *PC* through *SC*, as shown in figure 9.

A third coordinate system, the Rectangular Photo Coordinate System (R-Photo) is created with its origin at *PP*, its *X*–*Y* axial plane normal to the vector from *PC* through *SC* and its $+X$ axis aligned with the $+X$ axis of R-Spacecraft, as shown in figure 9. The *X*–*Y* plane of this coordinate system represents the image plane of the photograph.

5.3.4. *Auxiliary point calculations*

The calculations above employ a critical assumption that all photos are taken with the 'top of the image' oriented perpendicular to the vector from the *SN* towards *PC*, as shown in figure 9. To avoid non-uniform solar heating of the external surface, most orbiting spacecraft are slowly and continually rotated about one or more axes. In this condition a flight crew member taking a photo while floating in microgravity could orient the photo with practically any orientation relative to the horizon (see also figure 8(*b*)). Unfortunately, since these photos are taken with conventional handheld cameras there is no other information available which can be used to resolve the photo's rotational ambiguity about the optical axis, other then the photo itself. This is why the above assumption is used and the footprint computed by this calculator is actually a 'locator ellipse', which estimates the area on the ground what is likely to be included in a specific photograph (see figure 6). This locator ellipse is most accurate for square image formats and subject to additional distortion as the photograph format becomes more rectangular.

If the user wants a more precise calculation of the image footprint, the photo's rotational ambiguity about the optical axis must be resolved. This can be done in the calculator by adding data for an auxiliary point. Detailed instructions regarding how to prepare and use auxiliary point data in the computations are included in the 'How-To-Use' tab of the spreadsheet. Basically, the user determines which side of the photograph is top, and then measures the angle between the line from *PP* to the top of the photo and from *PP* to the auxiliary point on the photo (figure 9).

If the user includes data for an auxiliary point, a series of computations are completed to resolve the photo rotation ambiguity about the optical axis (i.e. the $+Z$ axis in R-Photo). A vector from the Auxiliary Point on the Earth (*AE*) through the photograph perspective centre (located at *SC*) is intersected with the photo image plane (*X*–*Y* plane of R-Photo) to compute the coordinates of the Auxiliary Point on the photo (*AP*) in R-Photo. A two-dimensional angle in the *X*–*Y* plane of R-Photo, from the $-X$ axis to a line from *PP* to *AP* is calculated, as shown in figure 9. The $-X$ axis is used as the origin of the angle since it represents the top of the photo once it passes through the perspective centre. The difference between the computed angle and the angle measured by the user on the photo resolves the ambiguity in the rotation of the photo relative to the principal line (figures 7 and 9). The transformations from R-Spacecraft and R-Photo are then modified to include an additional rotation angle about the $+Z$ axis in R-Photo.

5.3.5. *'Footprint' calculations*

The program next computes the coordinates of eight points about the perimeter of the image format (i.e. located at the four photo corners, plus a bisector point along each edge of the image). These points are identified in R-Photo based upon the photograph format size and then converted to R-Spacecraft. Since all computations are done in orthogonal coordinate systems, the R-Spacecraft to R-Photo

rotation matrix is transposed to produce an R-Photo to R-Spacecraft rotation matrix. Once in R-Spacecraft, a unit vector from each of the eight perimeter points, through the photo perspective centre (the same point as *SC*), is computed. This provides the coordinates for points about the perimeter of the image format, with their direction vectors in a common coordinate system with other key points needed to compute the photo footprint.

The next step is to compute the point of intersection between the spherical earth model and each of the eight perimeter point vectors. The scalar value for each perimeter point unit vector is computed using two-dimensional planar trigonometry. An angle γ is computed using the formula for the cosine of an angle between two included vectors (the perimeter point unit vector and the vector from *SC* to the centre of the Earth). Angle ψ is computed using the Law of Sines. Angle $\varepsilon = 180$ degrees $-\gamma - \psi$. The scalar value of the perimeter point vector is computed using ε and the Law of Cosines. The scalar value is then multiplied by the perimeter point unit vector to produce the three-dimensional point of intersection of the vector with Earth's surface in R-Spacecraft. The process is repeated independently for each of the eight perimeter point vectors. Aside from its mathematical simplicity, the value of arcsine (computed in step 2) will exceed the normal range for the sin of an angle when the perimeter point vectors fail to intersect with the surface of the earth. A simple test, based on this principle, allows the program to correctly handle oblique photos which image a portion of the horizon (see results for high oblique photographs in table 5).

The final step in the process converts the eight earth intersection points from the R-Spacecraft to R-Earth. The results are then converted to the standard geographic coordinate system and displayed on the 'Input-Output' page of the spreadsheet.

5.4. *Examples*

All three formulations were applied to the photographs included in this paper and the results are compared in table 5. Formulation 1 gives too small a value for distance across the photograph (*D*) for all but the most nadir shots, and thus serves as an indicator of the best theoretical case, but is not a good measure for a specific photograph. For example, the photograph of Lake Eyre taken from 276 km altitude (figure 2(*a*)) and the photograph of Limmen Bight (figure 7), were closest to being nadir views (offsets < 68 km or $t < 15^\circ$, table 5). For these photographs, *D* calculated using Formulation 1 was similar to the minimum *D* calculated using Formulations 2 and 3. For almost all other more oblique photographs, Formulation 1 gave a significant underestimate of the distance covered in the photograph. For figure 5(A) (the picture of Houston taken with a 40 mm lens), Formulation 1 did not give an underestimate for *D*. This is because Formulation 1 does not account for curvature of the Earth in any way. With this large field of view, assuming a flat Earth inflated the value of *D* above the minimum from calculations that included Earth curvature.

A major difference between Formulations 2 and 3 is the ability to estimate pixel sizes (*P*) in both directions (along the principal line and perpendicular to the principal line). For the more oblique photographs, the vertical estimate of *D* and pixel sizes is much larger than in the horizontal direction (e.g. the low oblique and high oblique photographs of Hawaii, figure 4, table 5).

For the area of Limmen Bight (figure 7), table 5 illustrates the improvement in the estimate of distance and pixel size that can be obtained by re-estimating the location of the *PC* with greater accuracy. Centre points in the catalogued data are

$\pm 0.5^\circ$ of latitude and longitude. When the centre point was re-estimated to $\pm 0.02^\circ$, we determined that the photograph was not taken as obliquely as first thought (change in the estimate of the look angle t from 16.9 to 12.8°, table 5). When the auxiliary point was added to the calculations of Formula 3, the calculated look angle shrank further to 11.0°, indicating that this photograph was taken at very close to a nadir view. Of course, this improvement in accuracy could have also led to estimates of greater obliquity, and corresponding larger pixel sizes.

We also tested the performance of the scale calculator with auxiliary point by estimating the corner and point locations on the photograph using a 1:1 000 000 Operational Navigational Chart. For this test, we estimated our ability to read coordinates from the map as $\pm 0.02^\circ$and our error in finding the locations of the corner points as $\pm 0.15^\circ$ (this error varies among photographs depending on the detail that can be matched between photo and map). For Limmen Bight (figure 7), the mean difference between map estimates and calculator estimates for four points was 0.31° (SD = 0.18, $n = 8$). For a photograph of San Francisco Bay (STS062-151-291) the mean difference between map estimates and calculator estimates for four points was 0.064° (SD = 0.18, $n = 8$). For a photograph of San Francisco Bay (STS062-151-291) the mean difference between map estimates and calculator estimates for eight points was 0.196° (SD = 0.146, $n = 16$). Thus in one case, the calculator estimates were better than our estimate of the error in locating corner points on the map. It is reasonable to expect that for nadir-viewing photographs, the calculator used with an auxiliary point can estimate locations of the edges of a photograph to within $\pm 0.3^\circ$.

5.5. *Empirical confirmation of spatial resolution estimates*

As stated previously, a challenge to estimating system-AWAR for astronaut photography of Earth is the lack of suitable targets. Small features in an image can sometimes be used as a check on the size of objects that can be successfully resolved, giving an approximate value for GRD. Similarly, the number of pixels that make up those features in the digitized image can be used to make an independent calculation of pixel size. We have successfully used features such as roads and airport runways to make estimates of spatial scale and resolution (e.g. Robinson *et al.* 2000c). While recognizing that the use of linear detail in an image is a poor approximation to a bar target, and that linear objects smaller than the resolving power can often be detected (Charman 1965), few objects other than roads could be found to make any direct estimates of GRD. Thus, roads and runways were used in the images of Houston (where one can readily conduct ground verifications, and where a number of higher-contrast concrete roadways were available), to obtain empirical estimates of GRD and pixel size for comparison with table 5.

In the all-digital ESC image of Houston (figure 3(*d*)) we examined Ellington Field runway 4-22 (centre left of the image) which is 2438.4 m × 45.7 m. This runway is approximately 6–7 pixels in width and 304–309.4 pixels in length, so pixels represent an distance on the ground 7–8 m. Using a lower contrast measure of a street length between two intersections (212.5 m = 21.1 pixels), a pixel width of 10.1 m is estimated. These results compare favourably with the minimum estimate of 8.1 m pixels using Formulation 1 (table 5). For an estimate of GRD that would be more comparable to aerial photography of a line target, the smallest street without tree cover that could be clearly distinguished on the photograph was 7.92 m wide. The smallest non-street object (a gap between stages of the Saturn rocket on display in

Table 5. Application of methods for estimating spatial resolution of astronaut photographs including Formulations 1, 2 and 3. Improved centre point estimates and auxiliary point calculations are shown for figure 7. Variables as used in the text: f, lens focal length; H, altitude; PC, photograph centre point; SN, spacecraft nadir point, D, distance covered on the ground; P, distance on the ground represented by a pixel; *Offset*., distance between PC and SN using the great circle formula, t, look angle away from SN.

					Formulation 1		Formulation 2				Formulation 3		
Photograph[1]	f (mm)	H (km)	PC[2]	SN	D (km)	P (m)	*Offset* (km)	t (°)	Range D (km)	P[3] (m)	t (°)	Range D (km)	P[4] (m)
Figure 2, Lake Eyre													
STS093-717-80	250	276	−29.0, 137.0	−28.4, 137.1	60.7	11.7	67.4	13.7	60.9–64.2	12.0	13.7	60.9–64.7	12.1, 12.4
STS082-754-61	250	617	−28.5, 137.0	−28.1, 135.0	135.7	26.1	201	18.0	138–148	27.5	17.9	138–153	27.7, 29.4
Figure 3, Houston													
STS062-97-151	40	298	29.5, −95.5	30.5, −95.4	410	78.8	112	20.5	348–589	90.1	20.5	351–638	95.1, 103.6
STS094-737-28	100	294	29.5, −95.5	28.3, −95.5	162	31.1	133	24.4	158–203	34.7	24.3	158–207	35.1, 39.0
STS055-71-41	250	302	29.5, −95.0	28.2, −93.7	66.4	12.8	192	32.5	73.6–84.7	15.2	32.2	73.9–85.7	15.4, 18.5
S73E5145	300	268[5]	29.5, −95.0		24.7	8.0							
Figure 4, Hawaii													
STS069-701-65	250	370	19.5, −155.5	20.4, −153.8	81.4	15.7	204	28.9	87.6–98.9	17.9	28.6	88.0–109	18.1, 21.0
STS069-701-70	250	370	21.0, −157.5	19.2, −150.7	81.4	15.7	738	63.4	149–233	36.7	60.7	148–556	39.4, 106.3
STS069-729-27	100	398	20.0, −156.6	20.5, −148.2	219	42.1	867	65.4	328–1310	158	62.4	323+	31.1, N/A

Table 5. (*Continued*).

Photograph[1]	*f* (mm)	*H* (km)	*PC*[2]	*SN*	Formulation 1		Formulation 2				Formulation 3		
					D (km)	*P* (m)	*Offset* (km)	*t* (°)	Range *D* (km)	*P*[3] (m)	*t* (°)	Range *D* (km)	*P*[4] (m)
Figure 7, Limmen Bight													
STS093-704-50	250	283	−15.0, 135.0	−15.0, 135.8	62.3	12.0	85.9	16.9	63.0–67.3	12.5	16.8	63.0–67.6	12.6, 13.2
PC Re-estimated			−14.733, 135.267				64.5	12.8	62.3–65.5	12.3	12.8	62.3–65.7	12.3, 12.7
Auxiliary Point[6]											11.0	62.3–65.1	12.3, 12.5
Figure 10, Near Austin, TX													
STS095-716-46	250	543	30.5, −97.5	28.6, −100.7	120	23.0	375	34.6	135–157	28.1	34.1	136–161	28.6, 36.0

[1]All photographs except one taken with Hasselblad camera so distance across the image, $d = 55$ mm; for S73E5145, taken with electronic still camera, $d = 27.65$ mm horizontal.

[2]*PC* and *SN* are given in the form (latitude, longitude) degrees, with negative numbers representing south and west. Accuracy of *PC* is ± 0.5 and *SN* is ± 0.1, as recorded in the Astronaut Photography Database, except where noted that centre point was re-estimated with greater accuracy.

[3]Calculated using the mean of the minimum and maximum estimates of *D*; Formulation 2 considers *D* in the direction perpendicular to the Principal Line only.

[4]Calculated in horizontal and vertical directions, but still assuming geometry of figure 6(B). First number is the mean of the minimum *D* at the bottom of the photo and the maximum *D* at the top of the photo (range shown in the table), and is comparable to Formulation 2. Second number is the mean of *D* estimated along the Principal line, and along the outside edge (range not shown).

[5]Altitude is approximate for mission as exact time photograph was taken and corresponding nadir data are not available. Lack of nadir data prevents application of Formulations 2 and 3.

[6]Auxilliary point added was −14.80 latitude, 135.12 longitude, −46.5° rotation angle; instructions for estimating the rotation angle parameter are contained as part of the scale calculator spreadsheet documentation.

a park at Johnson Space Center) that could clearly be distinguished on the photograph was 8.53 m wide.

For the photograph of Houston taken with a 250 mm lens (figure 3(C)), and digitized from second generation film at 2400 ppi (10.6 μm pixel^{-1}), Ellington Field runway 4-22 is 3 pixels in width and 161.3 pixels in length, so pixels represent 15.1–15.2 m on the ground. These results compare favourably with the minimum estimate of 15.2 m using Formulation 2, and 15.4–18.5 m pixels using Formulation 3 (table 5). For an estimate of GRD using an 8×8 inch print (1:3.69 enlargement) and $4\times$ magnification, the smallest street that could clearly be distinguished was 8.22 m wide, the same feature could barely be distinguished on the digitized image.

We also made an empirical estimate of spatial resolution for lower contrast vegetation boundaries. By clearing forest so that a pattern would be visible to landing aircraft, a landowner outside Austin, Texas (see also aerial photo in Lisheron 2000), created a target that is also useful for evaluating spatial resolution of astronaut photographs. The forest was selectively cleared in order to spell the landowner's name 'LUECKE' with the remaining trees (figure 10). According to local surveyors who planned the clearing, the plan was to create letters that were 3100 ft $\times$ 1700 ft (944.9 m $\times$ 518.2 m). Photographed at a high altitude relative to most Shuttle missions (543 km) with a 250 mm lens, Formula 3 predicts that each pixel would represent an area 28.6 m $\times$ 36.0 m on the ground (table 5). When original film was digitized at 2400 ppi (10.6 μm pixel^{-1}), letters correspond to 29.4×18.8 pixels for a comparable pixel size of 27–32 m.

6. Summary and conclusions

Astronaut photographs can be an excellent source of data for remote sensing applications. Best-case resolutions are similar to that for Landsat or SPOT with pixels as small as < 10 m. It was estimated that of images taken to date, 50.4% had lens and obliquity characteristics that make them potential candidates for remote sensing information. Digitized astronaut photographs can be overlaid with other satellite data using GIS (Eckardt *et al.* 2000), or used to fill in gaps in time series when other imagery is not available. As a source of public-domain information, they can be very useful for scientists who do not have access to satellite imagery either because of the expense of image acquisition (to the end user), or the computer systems needed for processing satellite images. These differences in image acquisition costs (to the user) are summarized in table 6.

Searching of the complete database of NASA astronaut photography, including low-spatial-resolution browse images, is available via the Web (Office of Earth Sciences 2000). This provides nearly global access for identifying images that will contribute to a specific scientific project. For the most detailed studies, digital products posted to the web will not be of sufficient quality. To date, we have made it a practice of digitizing small numbers of images when requested by scientists at no charge. Such requests (including a description of the project involved) can be made through the authors or using the contact information listed on the website. Investigators with needs for larger numbers of digital images have also been served through collaborative agreements.

In our experience, scientists that find the data most valuable are those in developing countries, those studying areas that have not usually been targets for the major satellites, those having difficulty in finding low-cloud images, those interested in constructing time series, or those interested in using a large number of images.

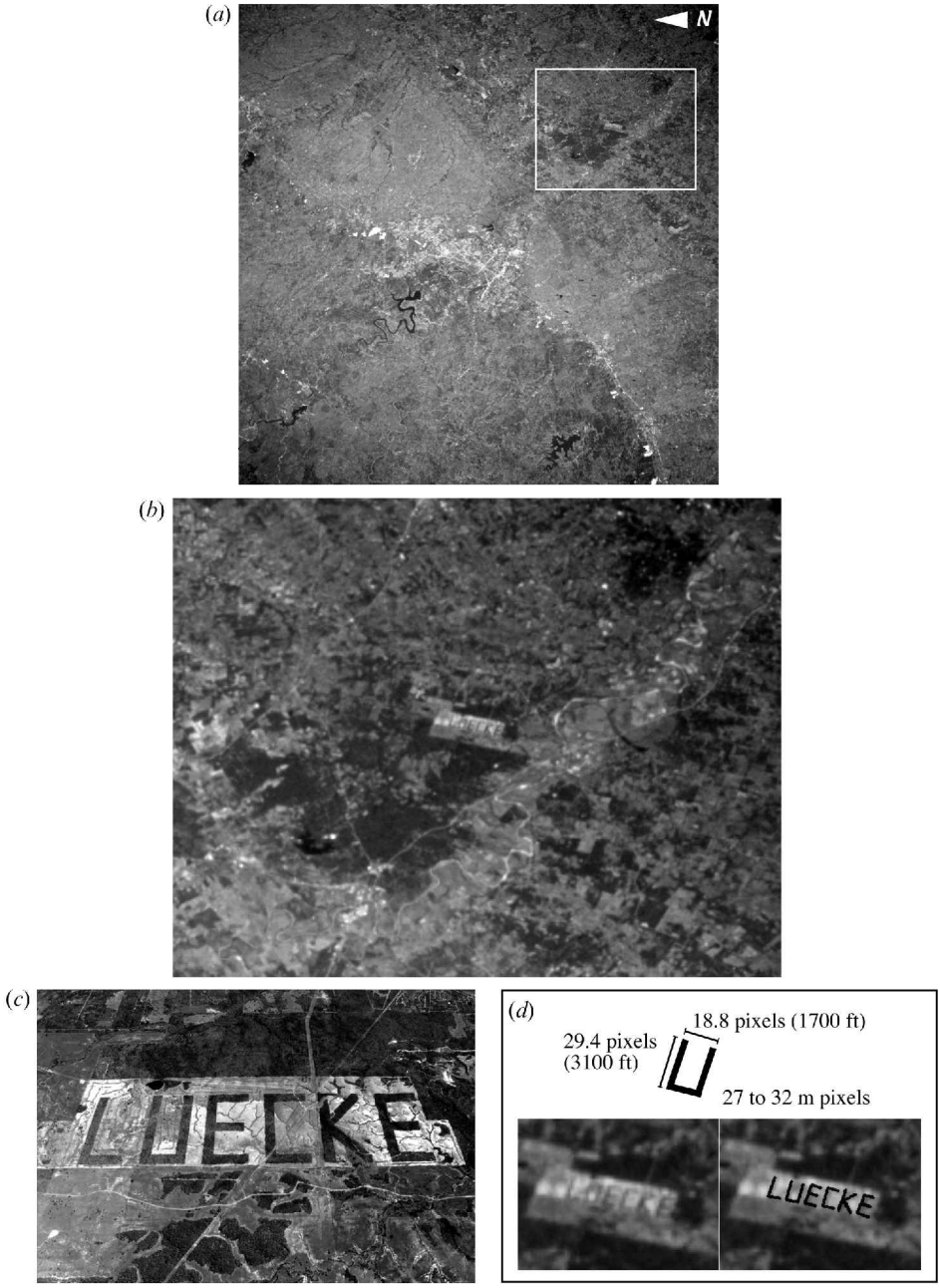

Figure 10. Patterns of forest clearing outside Austin, Texas serve as a test pattern for estimating spatial resolution. (*a*) Complete field of view for STS095-716-46 taken with a 250 mm lens from 543 km altitude (2 November 1998). (*b*) Detail of a portion of the frame. (*c*) Aerial photograph taken with an ESC (Kodak DCS620C) from an unknown altitude with zoom lens (2 March 2000, B. K. Diggs, Austin-American Statesman, used with permission). (*d*) Detail showing the limits of spatial resolution when the film was digitized at 2400 ppi (10.6 μm pixel^{-1}). The legend in the right-hand corner shows the field measurements for the letters (P. Tovar, Jr., personal communication) and the corresponding pixel size.

Table 6. Comparisons of characteristics of astronaut-directed photography of Earth with automatic satellite sensors[1]. Information compiled from webpages and press releases provided by the agent listed under 'References'.

	Astronaut-acquired orbital photography	Landsat			SPOT XS	AVHRR	CZCS	SeaWiFS
		MSS	TM	ETM+				
Length of record	1965–	1972–	1982–	1999–	1986–	1979–	1978–1986	1997–
Spatial resolution[2], m	9–65	79	30	30	20	1100 × 4000	825	1100–4400
Altitude, km	222–611	907–915	705	705	822	830–870	955	705
Inclination	28.5–51.6	99.2°	98.2°	98.2°	98°	81°	99.1°	98.3°
Scene size, km	Variable	185 × 185	185 × 170	185 × 170	60 × 60	2399 swath	1566 swath	2800 swath
Coverage frequency	Intermittent	18 days	16 days	16 days	26 days	2 × per day	6 days	1 day
Sun-synchronous orbit?[3]	No	Yes	Yes	Yes	Yes	Yes	Yes	Yes
View angles	Nadir, Oblique	Nadir	Nadir	Nadir	Nadir, Oblique	Nadir	Nadir, ±40°	Nadir, ±20°
Estimated product cost, per previously acquired scene (basic)	$0–25	$200	$425	$600	$1550–2300	0	0	0
References	NASA	EROS	EROS	EROS	SPOT	NOAA/NASA	NASA	NASA

[1]Abbreviations for sensors and government agencies are as follows: MSS Multi-spectral Scanner, TM Thematic Mapper, ETM+ Enhanced Thematic Mapper Plus, AVHRR Advanced Very-high Resolution Radiometer, CZCS Coastal Zone Color Scanner, SeaWiFS Sea-viewing Wide Field-of-view Sensor, SPOT Satellite pour l'Observation de la Terre, XS Multispectral mode, EROS Earth Resources Observation Systems Data Center, United States Geological Survey, Sioux Falls, South Dakota; NOAA National Oceanographic and Atmospheric Administration, NASA National Aeronautics and Space Administration.

[2]Additional detail is in table 2. Best-case nadir pixel size for a range of altitudes is included for orbital photographs.

[3]Determines degree of variability of lighting conditions among images taken of the same place at different times.

Because use of astronaut photography data is unfamiliar to most scientists and remote sensing experts, we have tried to provide a general synopsis of its major characteristics. One common source of confusion about the data arises from its variable spatial resolution. The issue of spatial resolution of astronaut photographs has been treated to a level of detail that has not been previously published. In addition, a primer of equations has been provided that can be used for calculating spatial resolution of a given photograph, and user-friendly methods have been incorporated for non-specialists to estimate spatial resolution of specific photographs (using tools on our Web interface or by downloading a spreadsheet). Although more variable than other types of satellite data, the information in the images can be extracted using familiar remote sensing techniques such as georeferencing and image classification. This makes the data source valuable for remote sensing applications in ecology and conservation biology, geography, geology and other related fields.

Acknowledgments

We thank the astronauts, cataloguers, and scientists whose efforts over the last 25 years have developed and preserved the remote sensing resource described in this paper. Barbara Boland served as a primary beta-tester for the Photo Footprint Calculator, and helped to improve its user interface. James Heydorn searched databases to help in compilation of summary statistics and figure 5; he also did the programming for our web display of photo footprints. Joe Caruana researched older film types. James C. Maida helped to produce the three-dimensional visualization in figure 9. Karen Scott provided comments on this manuscript and input into the section on window effects. Serge Andréfouët, Kamlesh P. Lulla, Edward L. Webb, and anonymous reviewers made constructive comments that greatly improved the manuscript.

References

Amsbury, D. L., 1989, United States manned observations of Earth before the Space Shuttle. *Geocarto International*, **4**(1), 7–14.

Arnold, R. H., 1997, *Interpretation of Airphotos and Remotely Sensed Imagery* (Upper Saddle River, NJ: Prentice Hall).

Baltsavias, E. P., 25 April 1996, Desktop publishing scanners. *OEEPE Workshop on the Application of Digital Photogrammetric Workstations, 4–6 March 1996, Lausanne*. http://dgrwww.epfl.ch/PHOT/workshop/wks96/art_1_4.html

Campbell, J. B., 1996, *Introduction to Remote Sensing*, 2nd edn (New York: Guilford Press).

Chamberlain, R. G., 1996, What is the best way to calculate the distance between two points? GIS FAQ Question 5.1. (revised in November 1997 and February 1998, 11 April 2000).

Charman, W. N., 1965, Resolving power and the detection of linear detail. *The Canadian Surveyor*, **19**, 190–205.

Colwell, R. N., 1971, *Monitoring Earth Resources from Aircraft and Spacecraft*, NASA SP-275 (Washington, DC: National Aeronautics and Space Administration).

Drury, S. A., 1993, *Image Interpretation in Geology*, 2nd edn (London: Chapman and Hall).

Eastman Kodak Company, 1998, *Kodak Aerochrome II Infrared film 2443, Kodak Aerochrome II Infrared NP film SO-134*, Aerial Systems Data Sheet, TI2161, Revised 3-98. Also available at http://www.kodak.com/US/en/government/aerial/technicalPubs/tiDocs/ti2161/ti2161.shtml (29 November, 1999).

Eckardt, F. D., Wilkinson, M. J., and Lulla, K. P., 2000, Using digitized handheld Space Shuttle photography for terrain visualization. *International Journal of Remote Sensing*, **21**, 1–5.

El-Baz, F., 1977, *Astronaut Observations from the Apollo-Soyuz Mission*, Smithsonian Studies in Air and Space, Vol. 1 (Washington, DC: Smithsonian Institution Press).

El-Baz, F., and Warner, D. M., 1979, *Apollo-Soyuz Test Project, Vol. II, Earth Observations and Photography*, NASA SP-412 (Houston, Texas: National Aeronautics and Space Administration, Lyndon B. Johnson Space Center).

Eppler, D., Amsbury, D., and Evans, C., 1996, Interest sought for research aboard new window on the world: the International Space Station. *Eos, Transactions, American Geophysical Union*, **77**, 121,127.

Estes, J. E., and Simonett, D. S., 1975, Fundamentals of image interpretation. In *Manual of Remote Sensing*, edited by R. G. Reeves (Falls Church, VA: American Society of Photogrammetry), pp. 869–1076.

Evans, C. A., Lulla, K. P., Dessinov, L. V., Glazovskiy, N. F., Kasimov, N. S., and Knizhnikov, Yu. F., 2000, Shuttle-*Mir* Earth science investigations: studying dynamic Earth environments from the *Mir* space station. In *Dynamic Earth Environments: Remote Sensing Observations from Shuttle-Mir Missions*, edited by K. P. Lulla and L. V. Dessinov John (New York: John Wiley & Sons), pp. 1–14.

Helfert, M. R., and Wood, C. A., 1989, The NASA Space Shuttle Earth Observations Office. *Geocarto International*, **4**(1), 15–23.

Helfert, M. R., Mohler, R. R. J., and Giardino, J. R., 1990, Measurement of areal fluctuations of Great Salt Lake, Utah, using rectified space photography. *Houston Geological Society Bulletin*, **32**, 16–19.

Jensen, J. R., 1983, Urban/suburban land use analysis. In *Manual of Remote Sensing*, 2nd edn, Vol. II, Interpretation and Applications, edited by J. E. Estes (Falls Church, VA: American Society of Photogrammetry), pp. 1571–1666.

Jones, T. D., Godwin, L. M., Wisoff, P. J., Amsbury, D. L., and Evans, C. A., 1996, Astronaut Earth observations during the Space Radar Laboratory missions. *Proceedings of the IEEE Aerospace Applications Conference, 3–10 February 1996, Snowmass at Aspen, Colorado* (Piscataway, NJ: Institute of Electrical and Electronics Engineers), Vol. 2, pp. 29–46.

Light, D. L., 1980, Satellite photogrammetry. In *Manual of Photogrammetry*, 4th edn, edited by C. C. Slama (Falls Church, VA: American Society of Photogrammetry), pp. 883–977.

Light, D. L., 1993, The National Aerial Photography Program as a geographic information system resource. *Photogrammetric Engineering and Remote Sensing*, **59**, 61–65.

Light, D. L., 1996, Film cameras or digital sensors? The challenge for aerial imaging. *Photogrammetric Engineering and Remote Sensing*, **62**, 285–291.

Lisheron, M., 6 March 2000, Jimmy Luecke thinks big. *Austin American-Statesman*, E1, E6.

Lowman, P. D., Jr., 1980, The evolution of geological space photography. In *Remote Sensing in Geology*, edited by B. S. Siegal and A. R. Gillespie (New York: Wiley and Sons), pp. 90–115.

Lowman, P. D., Jr., 1985, Geology from space: A brief history of geological remote sensing. In *Geologists and Ideas: A History of North American Geology*, edited by E. T. Drake and W. M. Jordan (Boulder, CO: Geological Society of America), pp. 481–519.

Lowman, P. D., Jr., 1999, Landsat and Apollo: the forgotten legacy. *Photogrammetric Engineering and Remote Sensing*, **65**, 1143–1147.

Lowman, P. D., Jr., and Tiedemann, H. A., 1971, *Terrain Photography from Gemini Spacecraft, Final Geologic Report*, Report X-644-71-15 (Greenbelt, MD: National Aeronautics and Space Administration, Goddard Space Flight Center).

Lulla, K., Evans, C., Amsbury, D., Wilkinson, J., Willis, K., Caruana, J., O'Neill, C., Runco, S., McLaughlin, D., Gaunce, M., McKay, M. F., and Trenchard, M., 1996, The NASA Space Shuttle Earth Observations Photography Database: an underutilized resource for global environmental geosciences. *Environmental Geosciences*, **3**, 40–44.

Lulla, K. P., and Helfert, M. R., 1989, Analysis of seasonal characteristics of Sambhar Salt Lake, India, from digitized Space Shuttle photography. *Geocarto International*, **4**(1), 69–74.

Lulla, K., Helfert, M., Evans, C., Wilkinson, M. J., Pitts, D., and Amsbury, D., 1993, Global geologic applications of the Space Shuttle Earth Observations Photography database. *Photogrammetric Engineering and Remote Sensing*, **59**, 1225–1231.

Lulla, K., Helfert, M., Amsbury, D., Whitehead, V. S., Evans, C. A., Wilkinson, M. J., Richards, R. N., Cabana, R. D., Shepherd, W. M., Akers, T. D., and Melnick,

B. E., 1991, Earth observations during Shuttle flight STS-41: Discovery's mission to planet Earth, 6–10 October 1990. *Geocarto International*, **6**(1), 69–80.

Lulla, K., Helfert, M. and Holland, D., 1994, The NASA Space Shuttle Earth Observations database for global change science. In *Remote Sensing and Global Change Science*, edited by R. A. Vaughan and A. P. Cracknell, NATO ASI Series, Vol. I24 (Berlin: Springer-Verlag), pp. 355–365.

Lulla, K., and Holland, S. D., 1993, NASA Electronic Still Camera (ESC) system used to image the Kamchatka Volcanoes from the Space Shuttle. *International Journal of Remote Sensing*, **14**, 2745–2746.

Luman, D. E., Stohr, C., and Hunt, L., 1997, Digital reproduction of historical aerial photographic prints for preserving a deteriorating archive. *Photogrammetric Engineering and Remote Sensing*, **63**, 1171–1179.

McRay, B., Scott, J., and Robinson, J. A., 2000, Technical applications of astronaut orbital photography: how to rectify multiple image datasets using GIS. Earth Observations and Imaging Newsletter, Office of Earth Sciences, Johnson Space Center.

Merkel, R. F., Salmon, J. G., and Sims, B. A., 1985, *Mission Ephemeris for the Maiden Voyage of the Large Format Camera (LFC) aboard the Space Transportation System (STS) Mission 41G*, Job Order 84-427, JSC-20383 (Houston, TX: Lyndon B. Johnson Space Center).

Mohler, R. R. J., Helfert, M. R., and Giardino, J. R., 1989, The decrease of Lake Chad as documented during twenty years of manned space flight. *Geocarto International*, **4**(1), 75–79.

Moik, J. P, 1980, *Digital Processing of Remotely Sensed Images*, NASA SP-431 (Washington, DC, National Aeronautics and Space Administration).

National Aeronautics and Space Administration, 1974, *Skylab Earth Resources Data Catalog*, JSC-09016 (Houston, TX: Lyndon B. Johnson Space Center).

Office of Earth Sciences, NASA-Johnson Space Center, 14 Mar. 2000. The Gateway to Astronaut Photography of Earth, http://eol.jsc.nasa.gov/SearchPhotos/

Rasher, M. E., and Weaver, W., 1990, *Basic Photo Interpretation: A Comprehensive Approach to Interpretation of Vertical Aerial Photography for Natural Resource Applications* (Fort Worth, TX: United States Department of Agriculture, Soil Conservation Service, National Cartographic Center).

Ring, N., and Eyre, L. A., 1983, Manned spacecraft imagery. In *Introduction to Remote Sensing of the Environment*, 2nd edn, edited by B. F. Richason, Jr. (Dubuque, Iowa: Kendall/Hunt Publishing Company), pp. 112–129.

Robinson, J. A., Feldman, G. C., Kuring, N., Franz, B., Green, E., Noordeloos, M., and Stumpf, R. P., 2000a, Data fusion in coral reef mapping: working at multiple scales with SeaWiFS and astronaut photography. *Proceedings of the 6th International Conference on Remote Sensing for Marine and Coastal Environments*, Vol. 2, pp. 473–483.

Robinson, J. A., Holland, S. D., Runco, S. K., Pitts, D. E., Whitehead, V. S., and Andréfouët, S., 2000b, High Definition Television (HDTV) Images for Earth Observations and Earth Science Applications, NASA TP-2000-210189 (Houston, TX: Lyndon B. Johnson Space Center).

Robinson, J. A., McRay, B., and Lulla, K. P., 2000c, Twenty-eight years of urban growth in North America quantified by analysis of photographs from Apollo, Skylab and Shuttle-*Mir*. In *Dynamic Earth Environments: Remote Sensing Observations from Shuttle-Mir Missions*, edited by K. P. Lulla and L. V. Dessinov (New York: John Wiley & Sons), pp. 25–42, 262, 269–270.

Robinson, J. A., Lulla, K. P., Kashiwagi, M., Suzuki, M., Nellis, M. D., Bussing, C. E., Lee Long, W. J., and McKenzie, L. J., In press, Astronaut-acquired orbital photography as a data source for conservation applications across multiple geographic scales. *Conservation Biology*.

Scott, K. P., 2000, *International Space Station Laboratory Science Window Optical Properties and Wavefront Verification Test Results*, ATR-2000(2112)-1 (Los Angeles, CA: Aerospace Corporation).

SIMONETT, D. S., 1983, The development and principles of remote sensing. In *Manual of Remote Sensing*, 2nd edn, Vol. I, Theory, Instruments and Techniques, edited by D. S. Simonett (Falls Church, VA: American Society of Photogrammetry), pp. 1–35.

SINNOTT, R. W., 1984, Virtues of the haversine. *Sky and Telescope*, **68**, 159.

SLATER, P. N., 1980, *Remote Sensing Optics and Optical Systems* (Reading, MA: Addison-Wesley).

SLATER, P. N., DOYLE, F. J., FRITZ, N. L., and WELCH, R., 1983, Photographic systems for remote sensing. In *Manual of Remote Sensing*, 2nd edn, Vol. I, Theory, Instruments and Techniques, edited by D. S. Simonett (Falls Church, VA: American Society of Photogrammetry), p. 231–291.

SLATER, R., 1996, *U.S./Russian Joint Film Test*, NASA Technical Memorandum 104817 (Houston, TX: Lyndon B. Johnson Space Center).

SMITH, J. T., and ANSON, A. editors, 1968, *Manual of Color Aerial Photography* (Falls Church, VA: American Society of Photogrammetry).

SNYDER, J. P., 1987, *Map Projections—A Working Manual*, U.S. Geological Survey Professional Paper 1395 (Washington, DC: U.S. Government Printing Office).

TOWNSHEND, J. R. G., 1980, *The Spatial Resolving Power of Earth Resources Satellites: A Review*, NASA Technical Memorandum 82020 (Greenbelt, Maryland: Goddard Space Flight Center).

UNDERWOOD, R. W., 1967, Space photography. In *Gemini Summary Conference*, NASA SP-138 (Houston, TX: Manned Spacecraft Center, National Aeronautics and Space Administration), pp. 231–290.

WEBB, E. L., EVANGELISTA, MA. A., and ROBINSON, J. A., 2000, Digital land use classification using Space Shuttle acquired orbital photographs: a quantitative comparison with Landsat TM imagery of a coastal environment, Chanthaburi, Thailand. *Photogrammetric Engineering and Remote Sensing*, **66**, 1439–1449.

WELCH, R., 1982, Spatial resolution requirements for urban studies. *International Journal of Remote Sensing*, **3**, 139–146.

WILMARTH, V. R., KALTENBACH, J. L., and LENOIR, W. B., editors, 1977, *Skylab Explores the Earth*, NASA SP-380 (Washington, DC: National Aeronautics and Space Administration).

WONG, K. W., 1980, Basic mathematics of photogrammetry. In *Manual of Photogrammetry*, 4th edn, edited by C. C. Slama (Falls Church, VA: American Society of Photogrammetry), pp. 37–101.